Journal of Geochemical Exploration 168 (2016) 49–64

Contents lists available at ScienceDirect

Journal of Geochemical Exploration

journal homepage: www.elsevier.com/locate/gexplo

Geochemistry, mineralogy, and isotope composition of Pb, Zn, and Cu in primary ores, gossan and barren ferruginous crust from the Perkoa base metal deposit, Burkina Faso

B. Kříbek [a,*], J. Zachariáš [b], I. Knésl [a], J. Míková [a], M. Mihaljevič [b], F. Veselovský [a], O. Bamba [c]

[a] Czech Geological Survey, Geologická 6, 152 00 Prague 5, Czech Republic
[b] Institute of Geochemistry, Mineralogy and Mineral Resources, Faculty of Science, Charles University in Prague, Albertov 6, 128 43 Prague 2, Czech Republic
[c] Université de Ouagadougou, B.P. 7021, Ouagadougou, Burkina Faso

ARTICLE INFO

Article history:
Received 9 February 2016
Revised 28 April 2016
Accepted 22 May 2016
Available online 28 May 2016

Keywords:
VHMS
Gossan
Ferruginous crust
Geochemistry
Isotopes of Pb
Cu
Zn
Burkina Faso

ABSTRACT

Gossan at the Perkoa deposit of stratabound lead and zinc ores (Burkina Faso) is composed of hematite, goethite, clay minerals, minerals of the brucite group and sulfates (corkite, alunite, natroalunite, hinsdalite and hidalgonite). Residual quartz contains inclusions of chalcopyrite, sphalerite and cinnabar. *Compared with the primary ores*, the gossan is especially enriched with As, Ba, Pb, P, and Sb. On the other hand, the contents of Ag, Co, Cu, Hg, Mo, Ni, and particularly Zn are significantly lower. However, *compared with the barren ferruginous crust* in the same area, the gossan is significantly enriched in most of chemical elements, namely As, Pb, Sb, and Zn and to lesser extent also in Ag, Ba, Cd, Mo, S, and Sr.

The isotopic composition of lead in massive primary ore and in gossan is practically identical. However, the isotopic composition of lead in disseminated ores, the bleached gossan envelope, and in mineralized soils in the Perkoa area is very variable and reflects mixing of ore and lithogenic lead. The $^{206/207}$Pb ratio in barren soils and ferruginous crusts is much higher compared with gossan and related altered rocks.

Compared to massive ore (δ^{65}Cu = +1.91 to +2.17‰ and δ^{66}Zn = +0.30 to +0.36‰, respectively), the gossan is depleted in heavy isotopes of copper and zinc (δ^{65}Cu = −0.02 to −0.58 and δ^{66}Zn = −0.10 to −0.88‰, respectively). The chemical weathering of sulfide-rich rocks thus gives rise to considerable variations in Cu isotopes (median: −2.36‰, $\Delta^{65}Cu_{gossan-massive\ ore}$), and minor changes in Zn isotopes (median: −0.73‰, $\Delta^{66}Zn_{\ gossan-massive\ ore}$). Isotopic composition of copper in gossan and lateritic soil sampled in the vicinity of gossan is similar but differs from barren laterite duricrust which is more depleted in the ^{65}Cu isotope. In zinc, no differences were proved between the δ^{66}Zn values in the gossan and those in the soil and ferruginous crust.

1. Introduction

Erosion and oxidation of massive sulfides when uplifted and exposed to the surface commonly leads to the formation of gossans, which dominate the space between the water table and the surface (Emmons, 1917; Andrew, 1984; Williams, 1990; Taylor and Thornber, 1992; Boyle, 1994; Skarpelis and Argyraki, 2009; Velasco et al., 2013). Here, surface water leached soluble elements and reprecipitates some of them forming secondary iron- and manganese-bearing (hydro)oxides and several minerals belonging to the jarosite supergroup (Taylor et al., 1980; Belogub et al., 2003; Butt et al., 2005; Atapour and Aftabi, 2007). Mineralogical and geochemical composition of gossan is basically due to the composition of primary ore (Taylor and Thornber, 1992; Butt et al., 2005). However, because of the different mobility of various target and pathfinder elements in the processes of weathering, the concentration of individual chemical elements in gossan usually do not correspond with the geochemical composition of primary ores. This can lead, especially during intense weathering in tropical climates, to incorrect conclusions about the nature of the primary mineralization based on the study of gossan (Butt et al., 2008).

A typical feature of post-Eocene development of West Africa has been an alternation of a wet climate favoring chemical weathering with periods of a dry climate convenient for mechanical erosion (Séranne, 1999). Such climatic variations have shaped a sequence of stepped lateritic paleo-land surfaces marking successive denudation stages (Michel, 1973; Grandin, 1976; Chardon et al., 2006; Burke and Gunnell, 2008). Common relics of each paleo-land surface in the sequence are commonly sealed by a ferruginous duricrust (ferricrete). During geochemical exploration it is usually impossible to distinguish remnants of ferruginous duricrust from gossan fragments straight in a

* Corresponding author.
E-mail address: bohdan.kribek@geology.cz (B. Kříbek).

http://dx.doi.org/10.1016/j.gexplo.2016.05.007
0375-6742/

hand specimen (Blot, 2004). Therefore, in order to identify gossan or gossan fragments enclosed in a ferruginous crust some mineralogical methods (e.g., identification of relict minerals of primary mineralization), studies of rock fabrics, and in particular geochemical methods are used (Butt et al., 2008).

Positive identification of gossan may also be made by using lead (Pb) isotopic ratios, due to the differences in isotopic signatures of host rocks, and potentially economic mineralization. Separation of Pb from U and Th to form an ore body at a particular time gives a unique signature of $^{208}Pb/^{206}Pb$, $^{207}Pb/^{206}Pb$ and $^{206}Pb/^{204}Pb$ isotopic ratios (Gulson and Mizon, 1979; Vaasjoki, 1985; Gulson, 1986).

Several studies have recently been devoted to the investigation of changes in the isotopic composition of copper (Cu) during the weathering of sulfide ores. These works were focused on the study of porphyry copper deposits (Mathur et al., 2010, 2012b; Mirnejad et al., 2010), on volcanic-hosted massive sulfide ores (VHMS; Mason et al., 2005), and on metalliferous black shales (Mathur et al., 2012a). In all cases It was observed that the copper in the products of weathering was to various degrees depleted or enriched in ^{65}Cu isotope relative to the primary ores (Braxton and Mathur, 2011). However, the isotopic composition of copper has never been used to distinguish gossan from a barren ferricrust in the same area.

The isotopic composition of zinc in gossans has not been studied yet. Experimental dissolution of sphalerite, however, showed that during the dissolution of sphalerite-rich rocks or sphalerite concentrate, the leachate is slightly enriched with ^{66}Zn, and therefore it is assumed that the weathering leads to depletion of the ^{66}Zn isotope in residual mineral phases (Fernandez and Borrok, 2009; Matthies et al., 2014).

The Paleoproterozoic Perkoa metamorphosed volcanic-hosted deposit (VHMS) in Burkina Faso is the only one known representative of this type of mineralization in West Africa. The deposit is unique because of the predominance of zinc over copper and lead. The Perkoa deposit is capped with gossan relics. Therefore, the objective of this paper is to (1) assess the differences in geochemistry and mineralogy of primary ores and the gossan in the Perkoa deposit, (2) to find the best geochemical pathfinders to help in distinguishing gossan from products of regional lateritic weathering, especially from the relics of ferruginous crusts, and (3) to verify the possibility of using the isotopic composition of Pb, Cu, and Zn in distinguishing gossan from barren ferruginous crusts in a terrain affected by a multi-stage lateritic weathering.

2. Geological setting of the Perkoa sulfide deposits

2.1. Primary ores

The Paleoproterozoic Baoulé-Mossi Domain (BMD) forms the major part of the Leo-Man Craton (Fig. 1) in West Africa and belongs to a polycyclic orogeny that originated around the Kénéma Man-Archean nucleus during the Eburnean orogeny (2200–2000 Ma; Liégeois et al., 1991; Milési et al., 1992; Ledru et al., 1994; Egal et al., 2002; Feybesse et al., 2006). The BMD is composed of granitoids and volcano-sedimentary greenstone belts, which host multiple gold and few base metal deposits (Milési et al., 1992; Béziat et al., 2008). The greenstone belts are comprised of two main sequences of rocks, from the bottom to top: (i) the Lower Birimian, mostly sedimentary sequence (B1), with tholeiitic basalts and common intercalations of tholeiitic volcano-sedimentary deposits and carbonates near the top and, (ii) the Upper Birimian, an essentially volcanic sequence (B2) occurring in separate areas and composed of basaltic or bimodal tholeiitic and late calcalkaline volcanic rocks (Milési et al., 1989; Ledru et al., 1991, 1994; Feybesse and Milési, 1994). The flysch-type, Paleoproterozoic Tarkwaian sediments (conglomerates and sandstones) overlie, partly discordantly, the folded Birimian sequences.

The Perkoa VHMS deposit forms a part of the Lower Birimian (B1) sequence (Fig. 2A). The deposit consists of two main ore bodies (locally called hanging wall and main ore body) and several satellite ore bodies, and ore disseminations, hosted by andesite, rhyolite and rhyodacite tuffs with intercalations of clinozoisite-actinolite and garnet-biotite schists with dykes of porphyric diorite and andesite (Schwartz and Melcher, 2003). The deposit is structurally overlain by silicified andesite/trachyandesite and carbonaceous schists. The intrusive quartz diorite/tonalite, which forms the footwall of the mineralization, was dated at 2175 ± 1 Ma (U-Pb zircon age; Schwartz and Melcher, 2003). The estimated ore reserves of the Perkoa are 6.3 Mt. with 14.5 wt.% Zn, 8.0 wt.% Ba,0.06 wt.% Pb, 24 ppm Ag, and 50 ppm Cu (Zida, 2002; MTMCI, 2015). The semitabular main ore body is 400 m long and has an average thickness of 10 m, whereas the hanging wall orebody has an average thickness of 4 m. Sulfide ores were metamorphosed during a regional thermal event. Peak metamorphic temperatures of >460 °C at pressures of >1 kbar are indicated by almandine-rich garnet, the presence of andradite, and geo-thermometers involving arsenopyrite and pyrrhotite (Schwartz and Melcher, 2003).

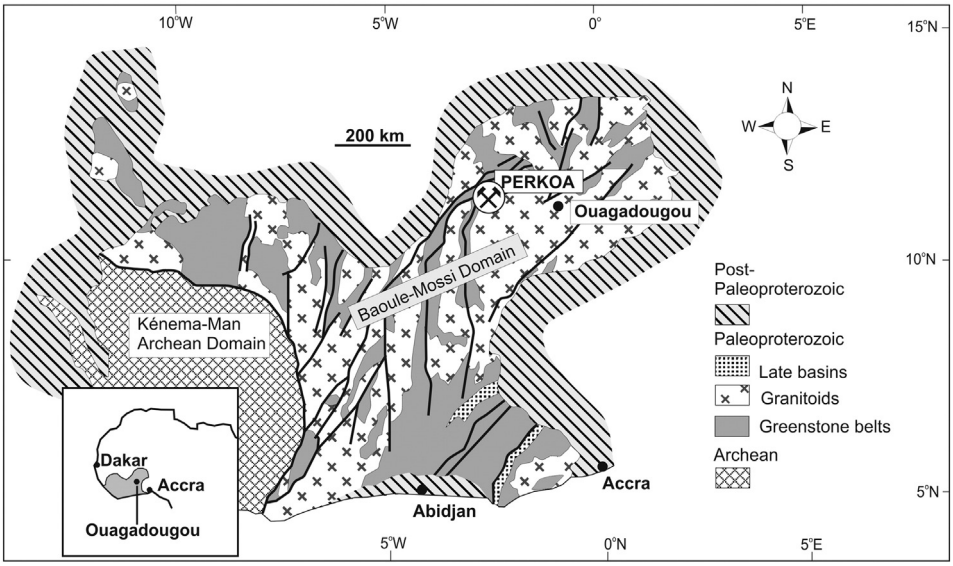

Fig. 1. Simplified geological map of the Leo-Man Craton (modified after the BRGM SIGAfrique map; Milési et al., 2004) with the study area indicated.

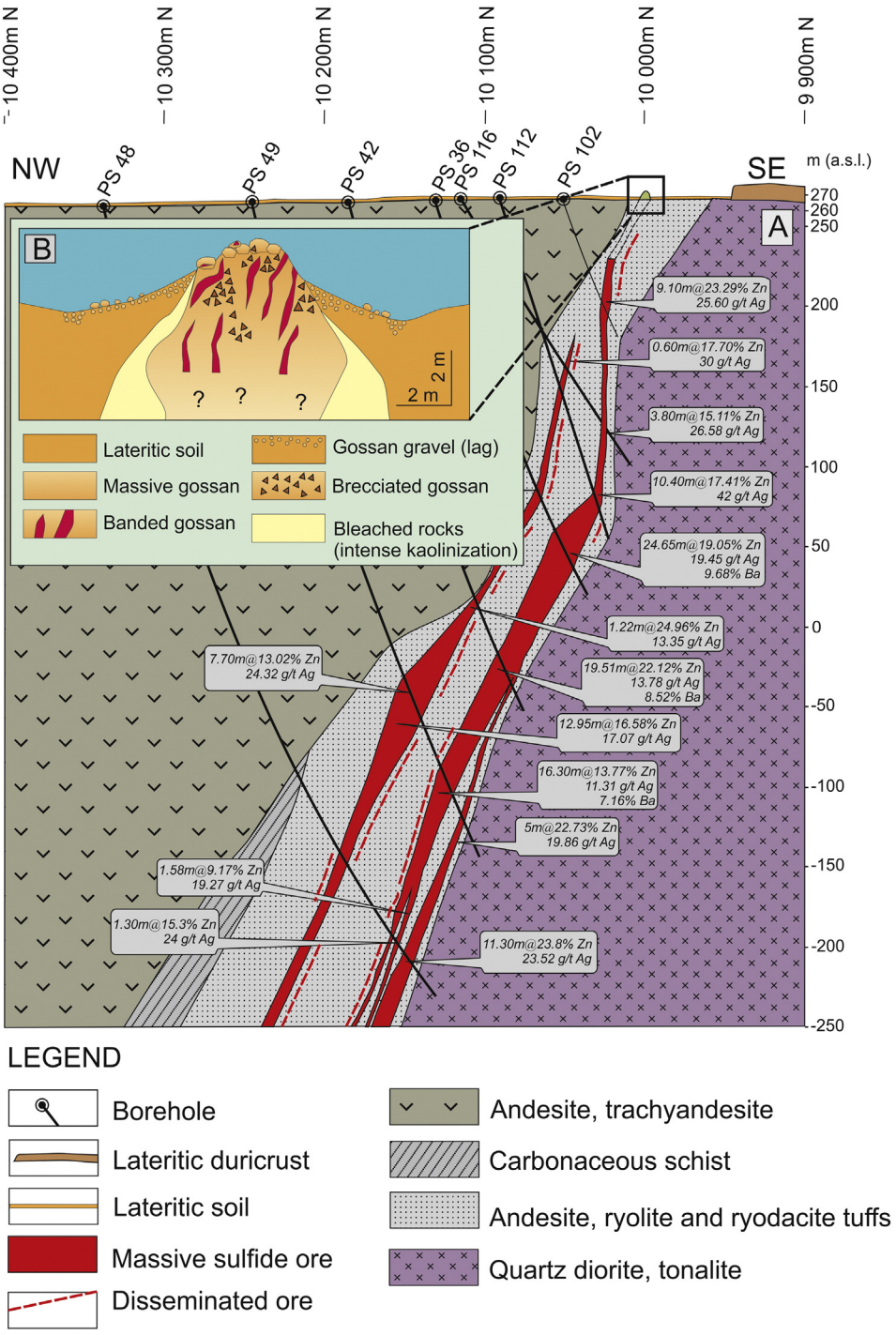

Fig. 2. Section No. 9975E of the Perkoa VHMS deposit, Burkina Faso (A), and a schematic illustration depicting the position and structure of gossan and its bleached envelope (B). With permission from Nantou Mining Limited.

2.2. Gossan and gossan bleached zone

The gossan is a surficial manifestation of weathering of massive sulfide ores (Fig. 2B). Individual gossan outcrops cover an area of 20 × 200 m, but the depth of the base of gossan body is not known. The gossan includes three lithofacies types: massive, banded, and brecciated. Massive gossan shows different fabrics ranging from cellular to colloform with many local transitions to box-work, stalactitic, or earthy forms. Crust precipitates of Fe (hydro)oxides line the vugs and pores. Banded gossans are relatively rare and represent the layering from the replaced original massive sulfides. Breccia gossan is the most common lithofacies. Gossan outcrops are within a few meters flanked with strongly bleached and argilitized rocks with sporadic accumulations of manganese minerals. These rocks are considered a manifestation of weathering of disseminated sulfides that accompany the massive sulfidic ore.

2.3. Ferruginous crust and soil

Two types of ferruginous crusts were found to occur in the studied area: Crusts that arose from the weathering of bedrock in situ (*autochthonous ferruginous crust*, *lateritic residuum*) and crusts that

originated through ferruginization of relocated products of weathering. The relocated products of weathering are mostly represented by ferruginized pediments that originated when the sheet erosion of the relief took place, or by sediments of old terraces or by alluvial sediments, which are the product of surface erosion by rivers and streams (*allochthonous ferruginous crust or ferricrete*). Both types of ferruginous crusts are usually covered with ferruginous gravel (lag) and in some places with a shallow soil profile.

The soil in the studied area is composed of a (1) a very thin (0–0.3 mm) litter layer, (2) a grey, 0–2 cm thick horizon containing small amount of humified organic matter, (3) a light grey unconsolidated sandy ochric horizon (bleaching horizon) up to 20 cm thick, and (4) a rusty-brown silty residuum of the parent rock with a more clay-rich layer up to 5 cm thick at its uppermost part. The soil can be classified according to the international FAO classification (FAO, 2006) as regosol.

3. Materials and methods

3.1. Sample collection and preparation

Several types of samples (Fig. 3) were collected at the Perkoa deposit. Besides samples of primary mineralization (massive and disseminated ores, borehole Ps 200), samples of gossan, and samples of bleached and strongly kaolinized zone in closest neighborhood of the gossan were also taken. Furthermore, soil samples were collected from a depth of 60–70 cm, both in the immediate neighborhood of the gossan outcrop (soils proximal to gossan) as well as soil samples taken at a distance of about 400 m west of the gossan exposure (distal soils). Soil samples were collected using a soil auger. Samples of ferruginous crust were taken from a hillside of morphologically pronounced escarpment, which lies about 400 m east of the gossan outcrop. A total of 58 samples (approx. 0.2 kg each) were collected from all types of materials. In the laboratory, the samples were ground, and homogenized in an agate mill to the finesse <0.063 mm. Polished thin sections and polished sections were prepared from samples of primary ores, gossan, and ferruginous crust for further microscopic and microprobe studies.

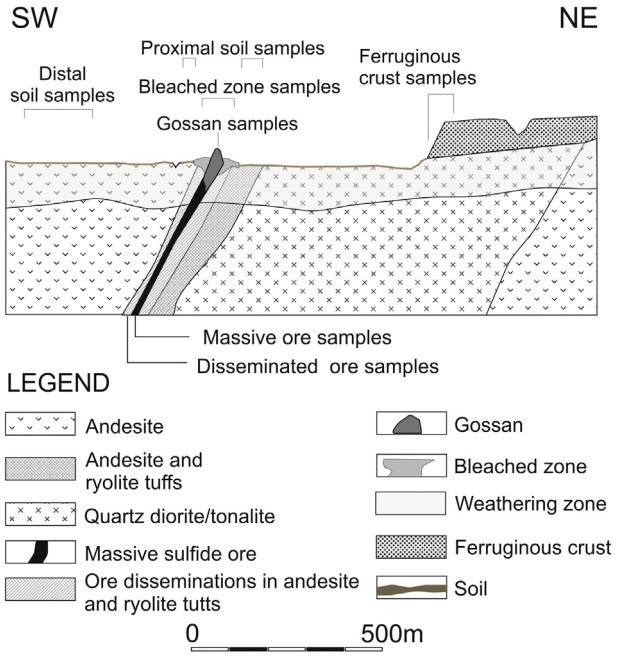

Fig. 3. Schematic section of the Perkoa area, Burkina Faso, and the location of collected samples.

3.2. Chemical analyses

Major components of rock samples were analyzed in the accredited Central Laboratories of the Czech Geological Survey in Prague. Samples of 0.2 g were dissolved in a solution of $HF/HNO_3/H_2SO_4$ at 200 °C, and evaporated to dryness. The residue was dissolved in a mixture of $HCl/HNO_3/H_2SO_4$ and H_3BO_3, and again evaporated to dryness. This evaporation residue was again dissolved in a solution of $HCl/H_2SO_4/Cs_2CO_3$, and the solution was analyzed using Flame Atomic Absorption Spectrometer Perkin Elmer 4000. The content of SiO_2 was determined by titration, using 1 N NaOH solution. Reliability of analyses as determined by in-home reference materials (RMS) was ±5%. The contents of CO_2 and total sulfur (S_{tot}) were established using an ELTRA CS instrument. The detection limits used for CO_2 were 0.02 wt.%, and for S_{tot} 0.01 wt.%. The relative percent difference (RPD) of CO_2 and S_{tot} determined using reference material (CRM 7001) were ±2.5% for CO_2 and ±2% for S_{tot}. Detailed analytical procedures are given in Dempírová and Vitková (2002).

Trace element concentrations were analyzed at Bureau Veritas Mineral Laboratories Ltd. (Vancouver, Canada; former Acme Analytical Laboratories). accredited under ISO 9002 by ICP-MS. The relative percent difference (RPD) using CRM OREAS 25a and OREAS 45e for most of chemical elements was excellent (±10% of the certified values) or good (±10–25%). For Ag, Cd, Re, Tb, Te, and Tm, the RPD were higher (>25) due to very low concentrations of elements in analyzed samples.

3.3. Mineralogical characterization

Determination of the mineralogical identity of rocks was attempted using a CamScan 3200 electron microprobe in SEM mode equipped with an energy dispersive analyzer LINK-ISIS. Analyses were undertaken using an accelerating voltage of 15 keV, and a beam current of 3 nA at the Czech Geological Survey or using an electron microscope (Vega-Tescan) equipped with an energy dispersive X-ray microanalyzer (X-max, Oxford Inst.) at the Faculty of Science, Charles University in Prague.

Quantititave analyses of Fe-, Mn-oxides and of minerals of the alunite supergroup were obtained using a Cameca SX 100 microprobe (WDS mode) at the laboratory of the Institute of Geology of the Czech Academy of Science. Operating conditions: accelerating voltage 15 keV, beam current 10 nA, beam size 2 μm.

Phase identification was carried out using a diffractometer Philips X'Pert System CuKα, 40 kV/40 mA, which is equipped with a secondary graphite monochromator. Records were obtained from unoriented samples (range 3–70° 2θ, step 0.05 2θ/3 s). The clay mineral fraction was studied using oriented samples (before and after saturation by ethylene glycol, range 2–50° 2θ, step 0.05 2θ, 2 s). Saturation of ethylene glycol was carried out in ethylene glycol vapors in a desiccator at 60 °C for 8 h. The pattern and expansibility of mixed-layer illite/smectite were determined by comparing the record with modeling the mixed-layer illite/smectite showing different expansibility using the NEWMOD program.

3.4. Whole rock lead isotopes ratios

The Pb isotopic compositions ($^{206}Pb/^{207}Pb$ and $^{208}Pb/^{206}Pb$ ratios) were determined using inductively coupled plasma mass spectrometry (ICP MS, XSeries 2, Thermoscientific) at the Institute of Geochemistry, Mineralogy and Mineral Resources, Faculty of Science, Charles University in Prague, under the conditions given elsewhere (Ettler et al., 2004; Mihaljevič et al., 2011). The solutions of mineralizates for isotopic determination were diluted to a concentration of <10 μg/l Pb. Correction for the mass bias was performed using NIST 981 (common lead) between measurements of the individual samples. The standard errors for measurement of the $^{206}Pb/^{207}Pb$ and $^{208}Pb/^{206}Pb$ ratios were <0.3% RSD and <0.4% RSD, respectively. The accuracy of the measurements were tested on reference materials BCR 2 (basalt; $^{206}Pb/^{207}Pb = 1.2007 \pm$

0.0007, $^{208}Pb/^{206}Pb = 2.0635 \pm 0.0016$) and AGV 2 (andesite; $^{206}Pb/^{207}Pb = 1.2085 \pm 0.0006$, $^{208}Pb/^{206}Pb = 2.0415 \pm 0.0013$) certified by the USGS (1998). The procedural blank was below 0.05 μg/l.

3.5. Whole rock copper and zinc isotopes ratios

Samples for Cu and Zn isotopic analyses were processed in the Ultraclean lab of the Czech Geological Survey in laminar flow hoods. Powdered samples were digested in acid in a microwave oven, and evaporated to dryness. The residue was dissolved in 2% solution of HNO_3, diluted, and analyzed using the ICP-MS. Copper and zinc fractions for isotope analysis were separated from acid-digested samples by ion exchange chromatography using the procedure described in Voldřichová et al. (2014) using 0.6 ml of AG–1MP 100–200 mesh (Bio-Rad) resin in a PE column (BioRad, total volume of 10 ml). The column was topped up with 0.1 M HCl and drained (repeated three times). The resin was then pre-conditioned with 6 ml of 8 M HCl. One milliliter of the sample in 8 M HCl was added. Matrix removal was performed by adding 1.5 ml of 8 M HCl. To separate Cu, a total amount of 11.5 ml of 6 M HCl was used. Subsequently, to separate Fe 11 ml of 3.5 M HCl was added. To collect Zn, 7 ml of 0.1 M HCl was added. An additional purification step for the Cu fraction employed small-volume columns packed with 0.15 ml BioRad AG MP-1 M anion-exchange resin (mesh 100–200) and 6 M HCl as elution media. The overall Cu–Fe–Zn separation recovery was better than 95% for all samples. The eluted Cu and Zn fractions were pooled for isotope analysis. All samples were analyzed in triplicate. Results are presented as weighted mean with standard deviation of these measurements. The reproducibility of standards measurements within whole analytical set (2σ) was 0.01 per mil for $\delta^{65}Cu$ and 0.03 per mil for $\delta^{66}Zn$.

Copper and zinc isotope analyses were carried out on a MC ICP MS Neptune (Thermo Fisher Scientific) instrument at the Czech Geological Survey. The $^{65}Cu/^{63}Cu$ ratios are reported in the $\delta^{65}Cu$ (‰) notation relative to the SRM NIST 976 standard. The mass bias of Cu measurements was corrected by standard-sample-standard bracketing using the SRM NIST 976. The $^{66}Zn/^{64}Zn$ ratios are reported in the $\delta^{66}Zn$ (‰) notation relative to the SRM NIST 683 standard. A $^{67}Zn–^{70}Zn$ double spike was used to correct the mass bias (Voldřichová et al., 2014).

3.6. Analytical data treatment

Summary statistics of the analytical data set were first calculated to evaluate the distributions. The frequency distribution for each set of elements was examined using histograms, Q–Q and P–P diagrams. Kurtosis and skewness were calculated using the S-Plus program version 4.5 (MathSoft Inc., Seattle, Washington, U.S.A., 1997). Since the statistical distribution of most variables determined by chemical analyses was not normal, non-parametric methods were used to evaluate the main statistical characteristics of the individual data populations using again the S-Plus program version 4.5.

Results of chemical analyses were used for the assessment and interpretation of the changes in major element contents during the weathering of primary ores. The immobile element concept was applied in this assessment and considerations. Within this concept, and supposing relatively homogeneous chemical and mineralogical composition of massive ores, the ratio between the studied element and immobile element concentration (Zr or Ti) in gossan and gossan bleached zone was compared with the same ratio in the fresh ore according to the following equation (Braun and Pagel, 1990):

$$\% \text{ change} = ((\chi/i)/(\chi_o/i_o)-1) * 100 \quad (1)$$

where: χ = content of the element in weathered rock, χ_o = content of the same element in fresh rock, i = content of Zr (Ti) in weathered rock, and i_o = content of Zr (Ti) in fresh rock.

4. Results

4.1. Mineralogy of primary ores

Massive sulfide ore is mainly composed of sphalerite, pyrite, hexagonal pyrrhotite, and minor magnetite and galena (grains <100 μm in size; Fig. 4AB). In addition, trace amounts of arsenopyrite, and silver-bearing tetrahedrite (freibergite), and Ti-phases were identified in some samples. Gangue minerals are represented by albite, calcite, quartz, barite, siderite, fluorite, and chlorite. The disseminated mineralization (Figs. 4CD and 5) is confined to muscovite-chlorite-quartz rocks (silicified tuffs or meta-exhalites). In muscovite-chlorite-quartz rocks, sphalerite occurs as isolated grains or accumulations together with pyrite in association with chlorite or muscovite in quartz gangue. Sphalerite, together with pyrite and magnetite, commonly rim garnet grains that are partly replaced by a mixture of muscovite and chlorite (Fig. 5ABC). Occurrence of gahnite (Zn-spinel) in mineralized rocks argues for pre-metamorphic origin of the mineralization (Fig. 5D).

4.2. Mineralogy of gossan

The gossan is mostly composed of hematite and goethite and minerals of the alunite supergroup. The amount of Mn-oxides is low. Clay minerals are represented by kaolinite and halloysite. Corroded and brecciated grains of quartz are common. Amorphous silica occurs as dissemination, usually in a mixture with clay minerals.

4.2.1. Goethite and hematite

Goethite (FeOOH) and hematite (Fe_2O_3) form either a massive rock matrix or micro-cockade layers that coat the vugs in the gossanized rock assemblage (Fig. 6). The gossan matrix is composed of a mixture of fine-grained goethite and relatively well crystallized needle-shaped hematite (Fig. 6AB). In pseudomorphs after sulfides, goethite relics are replaced by hematite which indicates that hematite is slightly younger than goethite (Fig. 6B). However, in other polished thin sections, the hematite is embedded in younger goethite suggesting that several stages of the goethite to hematite precipitation took place during the gossan evolution. Voids in gossanized rocks are rimmed by micro-cockade layers of goethite and hematite and fine-grained, nebulous, silica aggregates (Fig. 6CD). At these layers, goethite and hematite form spherical, botryoidal, mammillary textures, or replica textures after subautomorphous minerals of the jarosite supergroup.

Goethite contains up to 7 wt.% Al_2O_3 and SO_3. A rather high amount of Al_2O_3 in goethite suggests the Fe and Al substitution in the goethite structure or the presence of halloysite inclusions. An admixture of the Si, Ti, As, and P oxides attains up to 4 wt.%. Contents of ZnO and CuO are very low (<0.4 wt.%), whereas contents of PbO are very variable and range between <0.4 wt.% and 11 wt.%. The correlation between PbO and SO_3 contents in goethite may indicate an admixture of Pb-sulfates, presumably corkite. Positive correlation between SO_3 and P_2O_5 supports this possibility at least for goethite (Fig. 7). Compared to goethite, the contents of PbO (<2.97 wt.%) P_2O_5 (<0.40 wt.%) and SO_3 (<0.93 wt.%) in hematite are lower. Representative microanalyses of goethite and hematite are presented in Table 1S (electronic supplement).

4.2.2. Sulfates

Minerals of the alunite supergroup form numerous inclusions in hematite and goethite or are replaced by goethite in the rock matrix or form paragenetically youngest accumulations in voids and cracks (Fig. 8). The structural formula of jarosite supergroup minerals can be written as $DG_3(TX_4)_2(X')_6$ (Bayliss et al., 2010), where D represents a tetravalent, trivalent, divalent, monovalent cations (e.g. K^+, Na^+, Ba^+, Pb^{2+}, and H_3O^+) or partial vacancy; G represents a trivalent cations (chiefly Al^{3+} and Fe^{3+}); and minor divalent cations (e.g. Cu^{2+}, Zn^{2+}, Mg^{2+}); T is hexavalent (S, Cr), pentavalent (P, As, Sb) cations, and

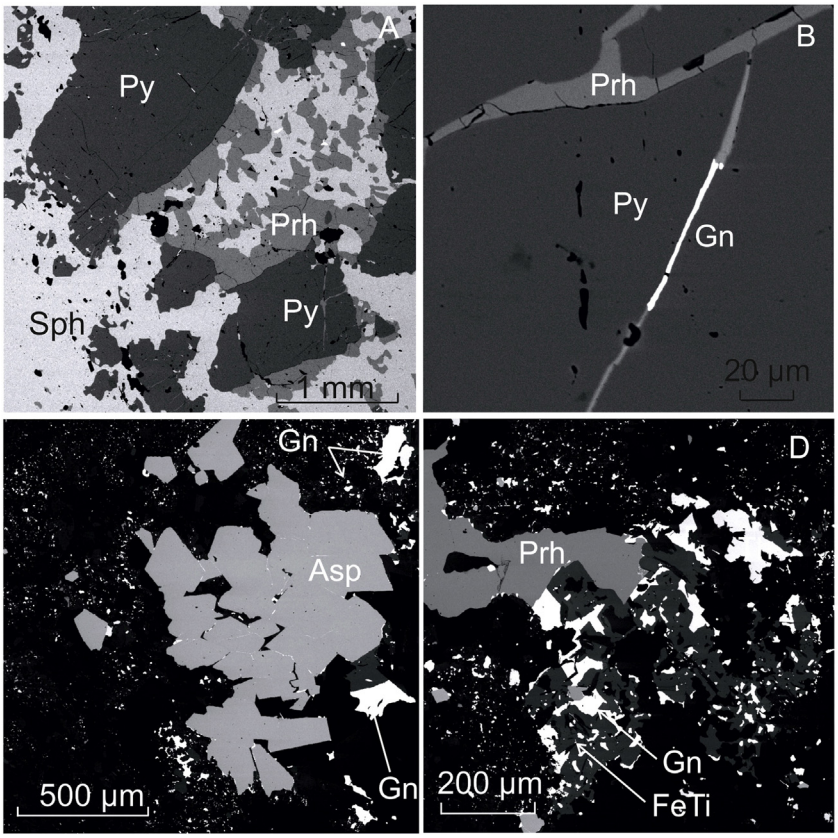

Fig. 4. Stratabound mineralization intersected by borehole Ps200, the Perkoa deposit (BSE images). A: Sample P280, depth: 280 m. The massive sphalerite (Sph), pyrite (Py), and pyrrhotite (Prh) ore. B: Massive ore, fracture in pyrite filled with pyrrhotite and galena. C: Sample Ps200, depth: 225 m. Disseminated mineralization in silicified metatuff. Arsenopyrite (Asp) aggregate associated with abundant satellite grains of galena (Gn). D: Sample Ps 200, depth: 250 m. Disseminated mineralization. Complex ore aggregate at the tip of altered Fe-Ti-O phase (Fe-Ti) consisting of pyrrhotite (Prh), and galena (Gn).

minor Si^{4+}; X/X′ is O, OH, minor F, and possibly H_2O. Corkite is a dominant mineral of the jarosite supergroup identified in the studied samples of gossan. However, together with corkite, the minor amounts of hindsdalite and hidalgonite were detected by microprobe (WD) analyses (Fig. 9). All minerals of the jarosite supergroup form individual crystals or less frequently twins, from 5 to 25 µm in size (Fig. 8E–H).

Images of secondary (SE) and/or back-scattered (BSE) electrons revealed micropores or vugs in central parts of many crystals of corkite

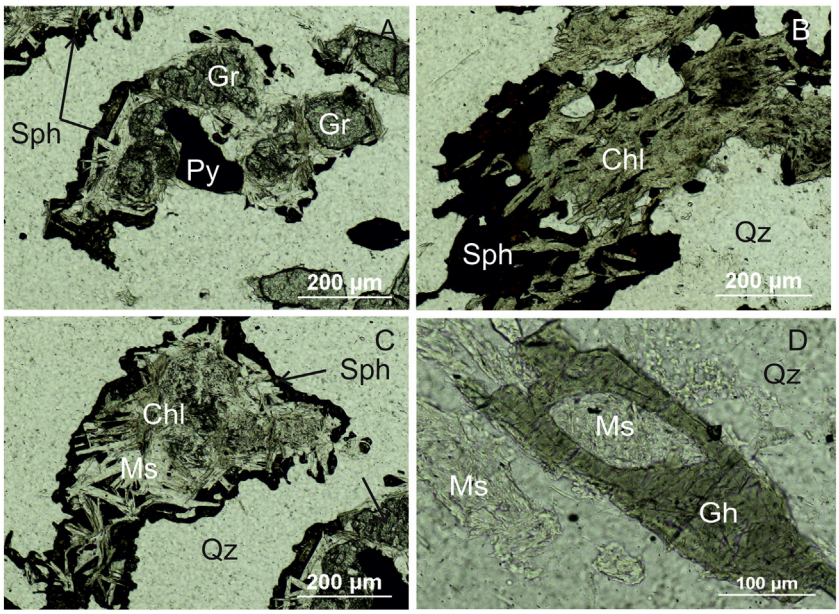

Fig. 5. Photomicrographs of polished thin sections of disseminated mineralization in borehole Ps200. A. Sphalerite (Sph) and pyrite (Py) rimming an aggregate of garnet grains (Gr) partly replaced by muscovite. B. Sphalerite (Sph) and chlorite (Chl) in quartz-rich groundmass. C. Sphalerite (Sph) rimming accumulations of muscovite, chlorite, and garnet remnants in quartz-rich (Qz) groundmass (transmitted light, without nicols). D: Gahnite (Zn-spinel, Gh) with muscovite inclusion (Ms) in quartz-muscovite groundmass (without nicols).

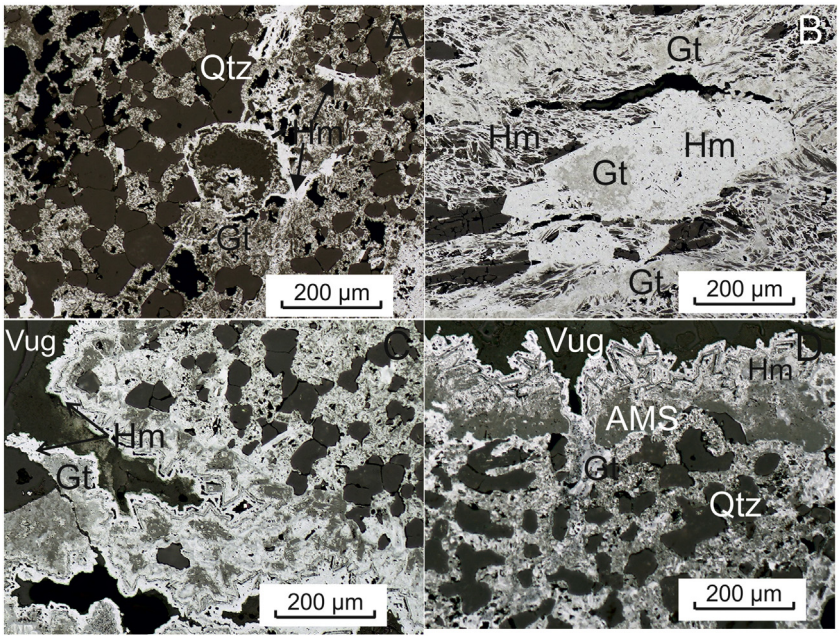

Fig. 6. Photomicrographs of polished thin sections of the gossan fabric. A. Massive fabric of gossan composed of a mixture of goethite (Gt) and slightly younger hematite (Hm) with corroded quartz grains (Qtz). B: Massive gossan fabric. Pseudomorph of Fe-minerals after sulfide grain (arsenopyrite?). Remnants of goethite (Gt, light grey) are enclosed in younger hematite (Hm, white). C. Porous fabric of gossan. Vugs in gossan are rimmed with a recurrence of goethite (Gt, light grey) and hematite (Hm, white) micro-cockade layers. D. Porous fabric of gossan. Zoned crystals of the jarosite supergroup minerals riming vugs in gossan are replaced by a mixture of hematite, goethite and amorphous silica (AMS).

(Fig. 8F). In addition to vugs, many crystals are chemically inhomogeneous; they frequently display chess-like textures or regular growth zones that differ mainly in PbO contents. The inhomogeneity of the minerals of the alunite supergroup results in the great variability of the total sum of analyzed oxides as well as in the non-stochiometric composition of sulfates studied. The great part of the non-stochiometry is due to an admixture of Fe (hydro)oxides, probably from adjacent hematite or goethite in the studied samples. Two microanalyses revealed, in addition to iron (hydro)oxides, an excess of Al_2O_3 which may be explained as due to an admixture of clay minerals, most probably halloysite or kaolinite. After subtraction of the Fe and Al admixture, the chemical composition of the alunite supergroup minerals revealed more or less stochiometric composition, with the exception of the D-site. Few microanalyses point to significant deficiency in the occupancy of the D-site (0.654 to 0.801 apfu); the majority of micro-analyses, however, approach more or less ideal occupancy in the range between 0.976 to 1.101 apfu (Fig. 10). Exceptionally, three microanalyses display an excess in the D-site occupancy in the range from 1.341 to 1.476 apfu. In this case, over 80% of the excess is at the charge of Pb. The occupancy of the T-site of the corkite by sulfur and phosporus ranges between the ideal ratio (~1, i.e. $S_{0.5}P_{0.5}$) and slight excess of sulfur (up to 2.3; i.e. $S_{0.7}P_{0.3}$). All corkite microanalyses display also minor admixture of As at the T-site (Fig. 9).

4.2.3. Mn (hydro)oxides

A complex rim of voids composed of micro-cockade layers of goethite and hematite in some polished sections intercalated with the Mn (hydro)oxides (Fig. 8D). However, the content of Mn (hydro)oxides is low and does not exceed 2 vol.% in general. Therefore, it was not possible to identify Mn (hydro)oxides using the XRD method. The wavelength-dispersive (WDS) microanalyses of Mn (hydro)oxides show an almost constant sum in the range from 76.73 to 82.73 wt.% (the average from 23 analyses is 79.61 wt.%). Therefore, it should be assumed that the main manganiferrous phase is pyrochroite ($Mn(OH)_2$), which ideally contains 22.25 wt.% H_2O. However, the occurrence of other manganiferous phases, for example poorly crystalline hydrous manganese minerals ("wad") cannot be excluded.

All Mn (hydro)oxides studied at the Perkoa deposit show substantial admixture of PbO (from 12.63 to 25.52 wt.%) and less important admixture of Fe_2O_3 (from 0.41 to 7.26 wt.%) and BaO (from 0.27 to 4.50 wt.%). The contents of BaO and PbO in Mn-oxides display a negative correlation (Fig. 11). Admixtures of other oxides are <0.4 wt.%, with an exception of ZnO, the contents of which range from 0.11 to 1.37 wt.% (Table 2S).

4.2.4. Clay minerals

Clay minerals (kaolinite and halloysite) constitute up to 15 vol.% of gossan. They form either pseudomorphs after rock-forming silicates or

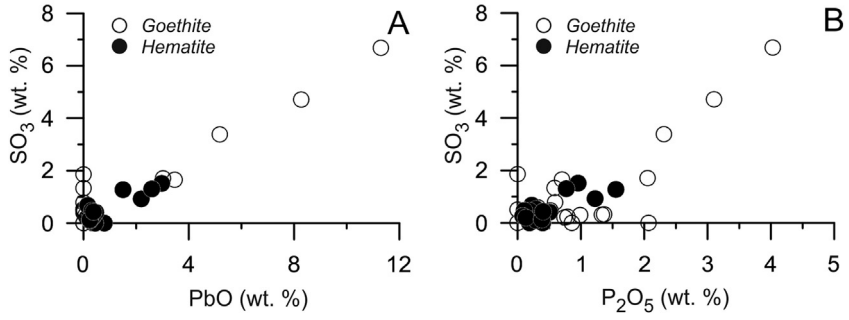

Fig. 7. Contents of PbO (A) vs. SO_3 (A) and P_2O_5 vs. SO_3 (B) in goethite and hematite. For representative analyses of goethite and hematite see Table 1S.

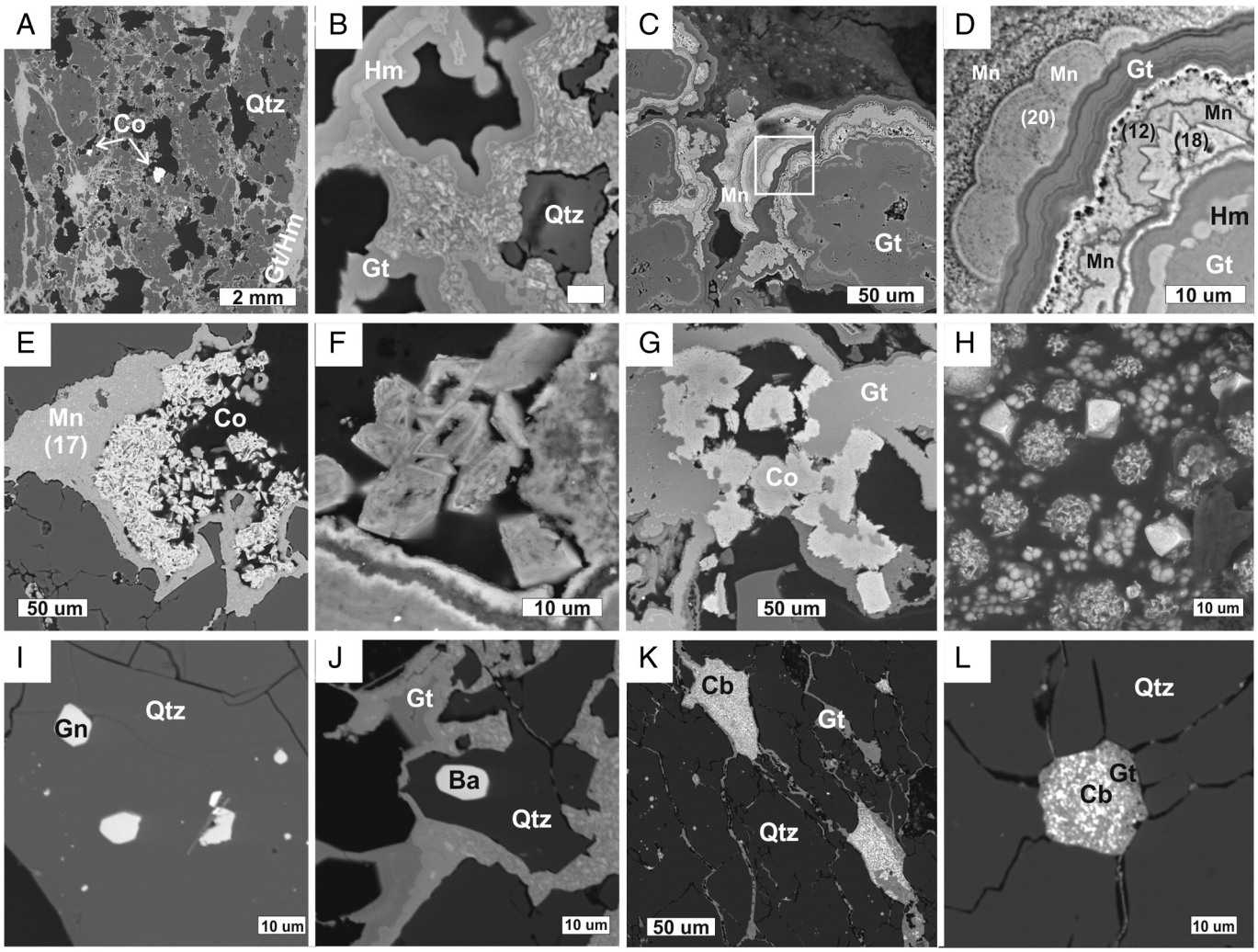

Fig. 8. Mineral phases in gossan, the Perka deposit (BSE images). A. Goethite and hematite veinlets penetrating the original quartz gangue. Free cavities are black, sulfates (corkite) are bright white. B. The rims of goethite enclosing lighter zones are enriched with Pb. This zone in the upper part of the BSE image is homogeneous, whereas in the central and the bottom parts it is strongly heterogenous. C. Kidney-shaped aggregates of goethite (darker) enclosing a thin zone formed by hematite. Kidney-shaped aggregates of Mn (hydro)oxides with markedly variable contents of Pb are younger than goethite. The oldest generation of Mn (hydro)oxides has a distinct crystalline character. D. Detail from the previous BSE image. Numbers in parentheses indicate admixture of PbO in wt.% bound in Mn (hydro)oxides. E. A rim of Mn (hydro)oxide with Pb admixture, which toward the cavity passes into a crystalline aggregate of corkite. F. Detail of individual crystals of corkite from the previous BSE image. Also striking is the zonal growth structure of crystals due to alternating areas richer or poorer in Pb, and the presence of open cavity in the center of corkite crystal. G. Massive and crystalline aggregates of corkite, which grow on goethite are also partly enclosed by this mineral. H. BSE image of the surface of free cavity in gossan. Kidney-shaped to spherical aggregates of goethite, spherical aggregates of crystallites of Fe-hydro-oxides, and several pseudocubic crystals of sulfates (corkite) can be seen. I-L. Group of BSE images showing primary ore minerals enclosed in an otherwise strongly weathered gossan material: I. inclusions of galena, J. barite inclusions, K and L. Relics of cinnabarite (bright dots) enclosed in goethite which forms filling in cracks. In both cases no mobilization of Hg (cinnabarite) into the surrounding fissures takes place. *Abbreviations*: Ba: barite, Cb: cinnabarite, Co: corkite, Gn: galena, Gt: goethite, Hm: hematite, Mn: Mn (hydro)oxides Qtz: quartz.

occur together with the cryptocrystalline silica, in the gossan groundmass. In strongly bleached and argilitized rocks that form the gossan envelope, illite, muscovite, and paragonite were identified using XRD, in addition to kaolinite.

4.2.5. Relict mineral phases in gossan

Relics of rock-forming or hydrothermal quartz grains enclose inclusions of chalcopyrite, pyrite, galena and barite which are not affected by supergenous alteration. The size of these inclusions ranges from 5 to 20 μm (Fig. 8IJ). At some places, cinnabar occurs together with goethite at the minute open cracks in quartz grains (Fig. 8KL). The chemical composition of cinnabar is stoichiometric, free of any admixture.

4.3. Mineralogy of the ferruginous crust

The lowermost part of the ferruginous crust studied at Perkoa (Fig. 3) is formed by an autochthonous crust (weathering residuum). The autochthonous crust is composed of a mixture of goethite, hematite, and clay minerals with preserved positions of quartz grains arranged in parallel to the original schistosity (Fig. 12A).

The rest of the profile represents an allochthonous ferruginous crust. The occurrence of rounded grains composed of Fe (hydro)oxides, clay minerals, and cryptocrystalline silica in fine-grained ferruginized rock matrix document that the upper part of the profile represents relocated products of weathering affected by an in situ ferruginization (Fig. 12B). Only hematite, goethite, cryptocrystalline silica, kaolinite, and small amount of Ti-oxides were identified in the rock matrix.

4.4. Geochemistry of primary ores vs. geochemistry of gossan

Both massive and disseminated primary ores predominantly contain Zn (14 to 35 wt.%). The amount of Pb (from 67 to 1181 ppm) and Cu (15–589 ppm) is much lower. Typical accompanying elements of Zn mineralization include Ag (7.6 to 169.3 ppm), As (105–210 ppm), Ba (75–190 ppm), Cd (0.67–1456 ppm) Mo (0.58–17.45 ppm), and Pb

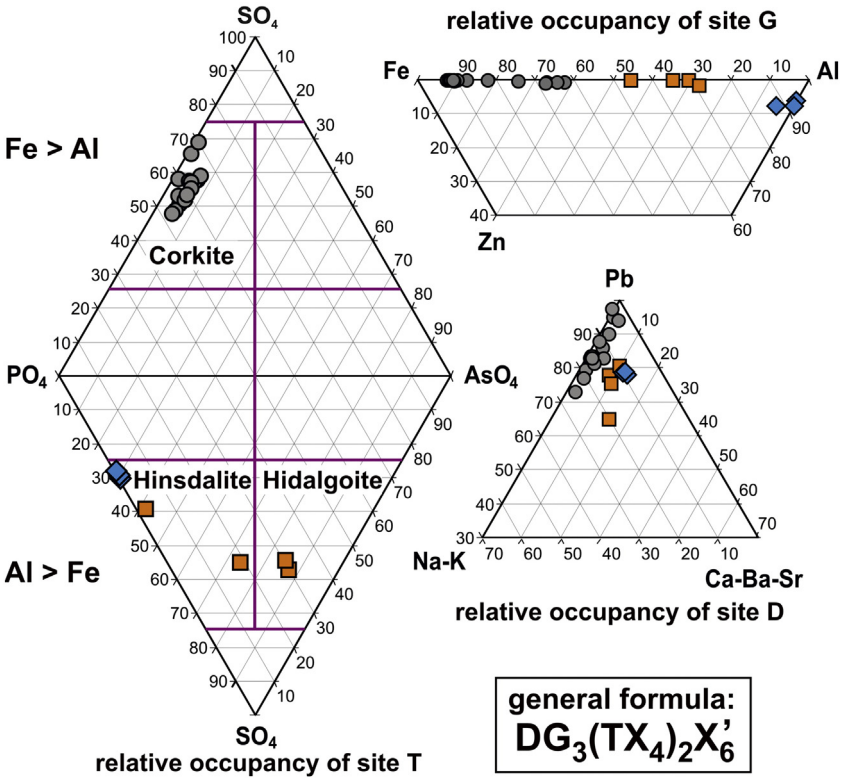

Fig. 9. Projection of microprobe analyses of studied sulfate phases into the classification diagram of the alunite supergroup after Scott (1987). Most analyses correspond to corkite, few to hindsdalite and hidalgonite.

(67–4049 ppm). Sulfur contents (S_{tot}) vary from 2.53 to 36.5 wt.%, depending on the amount of sulfides in ores (Table 3S).

In comparison with the primary ores the gossan rocks contain a much lower amount of Zn, but much higher concentrations of Pb (2702–31,042 ppm) and As (439–872 ppm; Table 3S). Due to the change in specific gravity of the primary ores during the process of weathering the contents of selected chemical elements in the primary ores and in gossan were normalized by contents of immobile chemical elements, i.e. titanium (Ti) and zirconium (Zr; Fig. 13). Upon normalization it is obvious that the gossan in relation to the primary ores is enriched in particular with Pb, As, Sb, Bi, and Ba. Conversely, the normalized contents of Cu, Zn, Ag, Ni, Co, Cd, In, Se, FeO, MgO, MnO, CaO, and S_{tot} are much lower in gossan compared with primary ores.

Gossan is relatively enriched in relation to the primary ores (expressed in ratios of individual elements to the content of Zr and Ti in the ore and gossan) also with light rare earths (La, Ce, Pr; Fig. 14).

4.5. Geochemistry of gossan vs. geochemistry of barren ferruginous crust

Concentrations of FeO, MnO, and the S_{tot} in gossan are much higher compared with the ferriginous crust, but conversely the contents of TiO_2 and Al_2O_3 are lower (Fig. 15A). The concentrations of other oxides vary within one order of concentration.

Gossan significantly differs from the ferruginous crust with higher contents of a wide range of trace elements. The contents (median values) of As, Pb, Sb, and Zn are by two orders of magnitude higher in gossan than in the ferruginous crust, and the contents of Ag, Ba Cd, Mo, and Sr are higher by one order of magnitude (Fig. 15B). On the contrary, the ferruginous crust in comparison with gossan has by order of magnitude higher contents of Sc. Also higher are contents of Nb, Ni, and Zr (not shown in Fig. 15B). Representative chemical analyses of gossan and ferruginous crust are given in Table 3S. Basic statistical data on the distribution of individual chemical elements and their oxides are shown in Table 4S.

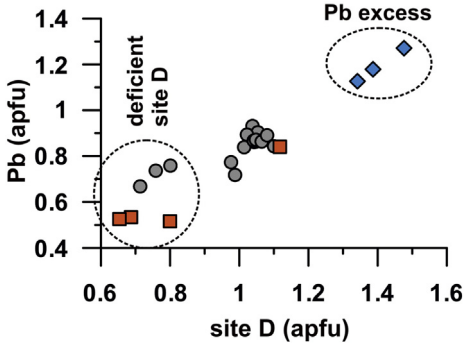

Fig. 10. Correlation between the Pb content and the occupancy of site D (ideal occupancy is equal to 1) of studied sulfate phases. Symbols are the same as in Fig. 9.

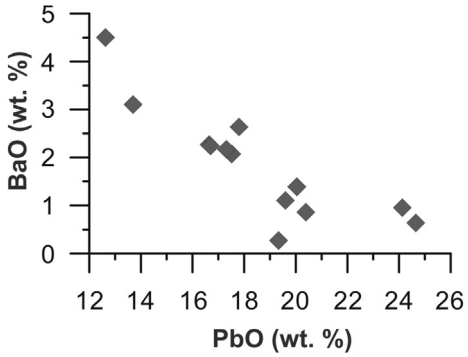

Fig. 11. Correlation between the BaO and PbO contents in Mn (hydro)oxidic phase.

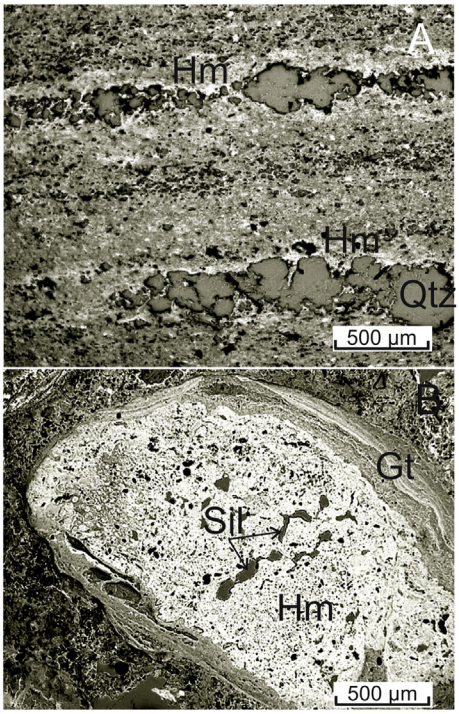

Fig. 12. Textures of the barren ferruginous crust studied at the Perkoa area. A. The lowermost part of the profile. Autochthonous ferruginous crust composed of a mixture of hematite, goethite, clay minerals, and positions of corroded quartz grains arranged in parallel to the original schistosity of the bedrock. B. The upper part of the crust is composed of rounded grains of hematite coated with goethite in fine-grained rock matrix. The occurrence of rounded grains confirms that the upper part of the profile represents relocated product of weathering affected by in situ ferruginization. *Abbreviations*: Gt: Goethite, Hm: Hematite, Qtz: Quartz, Sil: cryptocrystalline silica.

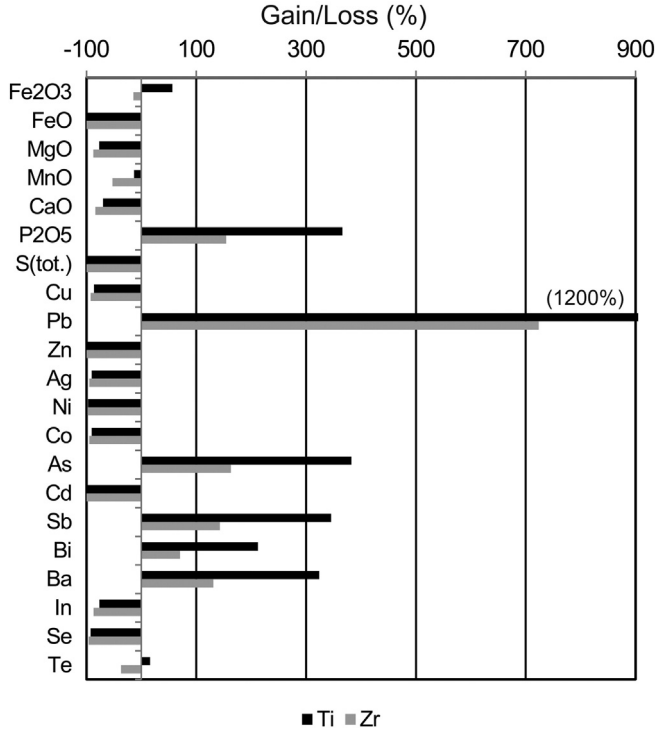

Fig. 13. Changes (in %) in the contents of selected chemical elements/oxides in gossan in relation to their contents in primary ores. Calculation is based on Ti and Zr as immobile elements. Median values of primary ores ($n = 7$) and gossan ($n = 8$) were used for the calculation.

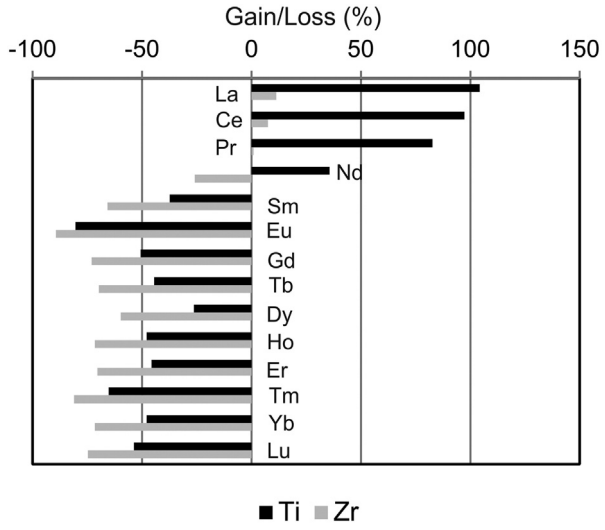

Fig. 14. Changes (in %) in the contents of rare earth elements (REE) in gossan in relation to their contents in primary ores. Calculation is based on Ti and Zr as immobile elements. Median values of primary ores ($n = 7$) and gossan ($n = 8$) were used for the calculation.

4.6. Izotope geochemistry of primary ores, gossan and products of regional weathering

4.6.1. Lead isotopes

Isotopic composition of Pb in massive primary ore (whole rock analyses, mean $^{206}Pb/^{207}Pb = 0.98 \pm 0.002$, mean $^{208}Pb/^{206}Pb = 2.34 \pm 0.006$) is very homogeneous and practically identical with that in the

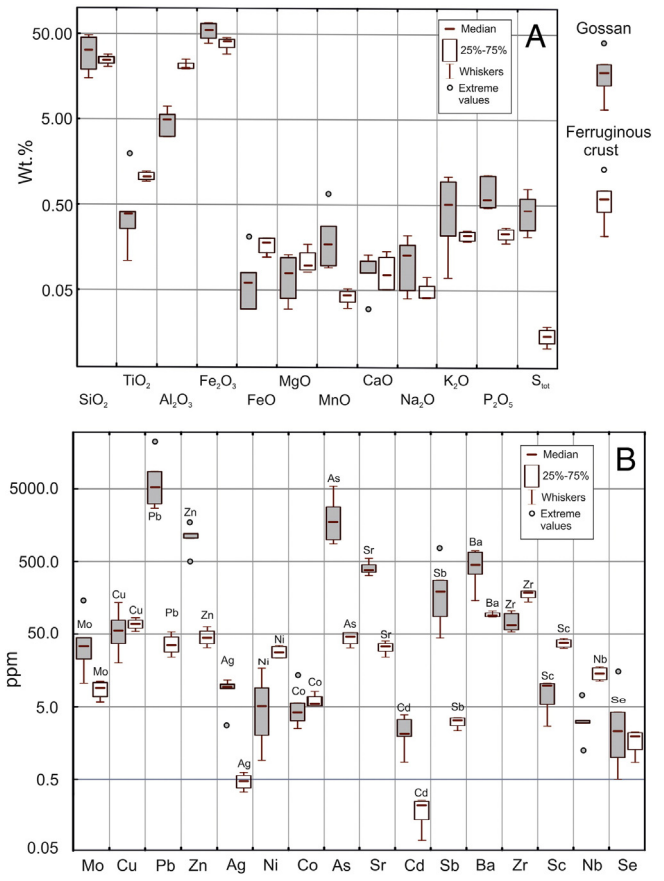

Fig. 15. Contents of selected major elements (A) and also trace elements (B) in gossan ($n = 16$) and in the barren ferruginous crust at the Perkoa deposit ($n = 24$).

gossan (mean $^{206}Pb/^{207}Pb = 0.98 \pm 0.003$, mean $^{208}Pb/^{206}Pb = 2.34 \pm 0.007$; Table 1, Fig. 16). However, the isotopic composition of disseminated primary ore is more variable ($^{206}Pb/^{207}Pb = 0.98–1.05$ and $^{208}Pb/^{206}Pb = 2.26–2.34$ respectively) which argues either for a primary variability of the isotopic composition of lead bound in ore or for mixing two sources of Pb (the ore and host rock lead). The isotopic composition of Pb in the bleached gossan envelope in principle copies the isotopic composition of massive or disseminated primary ores.

The isotopic composition of Pb in the barren ferruginous crust differs from the isotopic composition of lead in primary ores, gossan, and in the bleached argilitic gossan envelope (mean $^{206}Pb/^{207}Pb = 1.11 \pm 0.002$, $^{208}Pb/^{206}Pb = 2.16 \pm 0.006$), which allows us to distinguish gossan and argilitized rocks occurring in the neighborhood of gossan from products of regional weathering. The ratios of $^{206}Pb/^{207}Pb$ a $^{208}Pb/^{206}Pb$ (1.11 ± 0.002 and 2.16 ± 0.006 respectively) in soils in the immediate vicinity of gossan are rather close to those characteristic of the ore Pb, while the same ratio in the distal soils with low lead content, is close to isotopic ratios of $^{206}Pb/^{207}Pb$ a $^{208}Pb/^{206}Pb$ in the barren ferruginous crust.

4.6.2. Copper and zinc isotopes

Compared with primary massive or disseminated ore (whole rock analyses, $\delta^{65}Cu = +0.21$ to $+2.17‰$) the Cu in gossan and in the gossan bleached envelope in its closest vicinity is depleted in the heavy isotope ($\delta^{65}Cu = -0.02$ to $-0.69‰$; Table 2, Fig. 17A). However, Cu in gossan is less depleted in the heavy isotope compared with Cu in the ferruginous crust ($\delta^{65}Cu = -1.68$ to $-2.81‰$). The isotopic composition of Cu in soils is variable and ranges within values characteristic of gossan and the ferruginous crust. In comparison with copper, the differences in Zn isotopes confined to primary ores, gossan, and the ferruginous crust are much smaller. Yet it is clear that compared with the primary ores ($\delta^{66}Zn = +0.17$ to $+0.63‰$; Table 2, Fig. 17B) the Zn in both the gossan and analyzed soils, and also in the ferruginous crust is depleted in its heavy isotope. However, the isotopic composition of Zn in gossan and the bleached and argilitized zone around gossan ($\delta^{66}Zn = -0.88$ to $+0.34‰$) does not differ much from its isotopic composition in the ferruginous crust ($\delta^{66}Zn = -0.05$ to $-1.05‰$) and in soils ($\delta^{66}Zn = -0.03$ to $-0.63‰$).

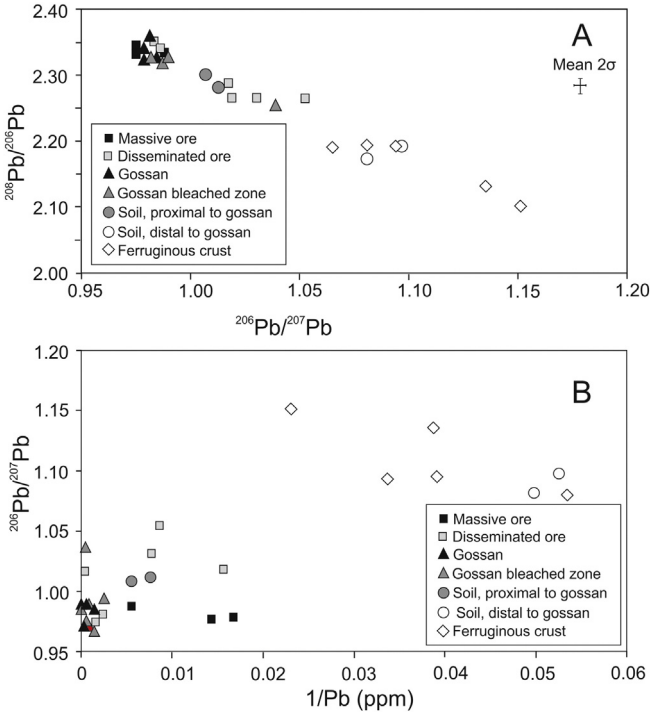

Fig. 16. Three isotopes plot ($^{206}Pb/^{207}Pb$ vs. $^{208}Pb/^{206}Pb$) for isotopic composition of massive and disseminated ore, gossan and the gossan bleached zone, soil and barren ferruginous crust (A) and Pb concentrations vs. $^{206}Pb/^{207}Pb$ plot in the Perkoa area (B).

Table 1
Concentration of Pb and Pb isotopic composition ($^{206}Pb/^{207}Pb$ and $^{208}Pb/^{206}Pb$, respectively) of analyzed samples of primary ore, gossan, gossan bleached envelope, soils and barren ferruginous crust at the Perkoa area, Burkina Faso.

Sample type/sample code	Pb(ppm)	$^{206}Pb/^{207}Pb$	2σ*	$^{208}Pb/^{206}Pb$	2σ*
Massive sulfidic ore					
PS200/250.5	182.6	0.987	0.003	2.332	0.012
PS200/280.0	60.2	0.977	0.005	2.344	0.014
PS200/281.0	70.0	0.976	0.004	2.335	0.012
Disseminated sulfidic ore					
PS200/333.5	64.3	1.017	0.005	2.288	0.010
PS200/225.9	1733.0	1.019	0.006	2.268	0.010
PS200/270.3	986.3	0.978	0.004	2.345	0.012
PS200/297.8	399.7	0.981	0.005	2.338	0.015
PS200/333.5	129.7	1.030	0.003	2.264	0.012
PS200/286.5	115.6	1.052	0.006	2.264	0.010
Gossan					
BFPE-2	8633.8	0.979	0.008	2.340	0.014
BF-PE-8-C	13,104.0	0.980	0.006	2.340	0.015
BF-PE-8-B	31,042.0	0.980	0.005	2.346	0.016
BF-PE-8-A	17,366.0	0.983	0.006	2.336	0.012
Bleached envelope of gossan					
BF-PE-23A	3566.3	0.978	0.008	2.344	0.016
BF-PE-21-C	2212.0	0.978	0.005	2.346	0.010
BFPE21E	5377.0	1.039	0.005	2.252	0.012
BF-PE-24A	2702.3	0.982	0.006	2.330	0.019
Soil (proximal to gossan)					
BFPE1/1	131.0	1.012	0.065	2.288	0.092
BFPE1/2	173.0	1.009	0.006	2.295	0.017
Soil (distal to gossan)					
BFPE1/40	20.0	1.082	0.013	2.184	0.024
BFPE1/41	19.0	1.096	0.006	2.190	0.010
Ferruginous crust					
BFPE9	18.8	1.082	0.006	2.188	0.014
BFPE10	25.8	1.136	0.004	2.129	0.012
BFPE11	43.3	1.151	0.006	2.098	0.013
BFPE12	25.6	1.094	0.005	2.188	0.011
BFPE8	30.0	1.094	0.004	2.185	0.010

* 2σ: Standard deviation. Analyses were performed in triplicate.

Spearman's correlation analysis of ores, gossan and barren ferruginous crust revealed a significant positive correlation at a probability level $p < 0.001$ (99.9%) between $\delta^{65}Cu$ values and concentrations of CaO (0.78), S_{tot} (0.95), Cu (0.66), Zn (0.85), Ag (0.72), Cd (0.91) Se (0.70) and $\delta^{66}Zn$ values (0.61). Significant negative correlation at the same probability level were found between $\delta^{65}Cu$, and elements or their oxides enriched in the barren ferruginous crust: TiO_2 (−0.78), Al_2O_3 (−0.78), Th (−0.89), V (−0.83), Cr (−0.82), Zr (−0.97), Sc (−0.72), Ta (−0.83), Nb (−0.85) and Ga (−0.86).

As for $\delta^{66}Zn$ values, significant positive correlation was found between Cu (0.62), Zn (0.73), Co (0.71), Cd (0.61), and $\delta^{65}Cu$ values (0.85), while negative significant correlation exists between $\delta^{66}Zn$ values and Fe_2O_3 (−0.64), P_2O_5 (−0.63), Th (−0.75), V (−0.66), Cr (−0.71), Zr (−0.64), Ta (−0.62), Nb (−0.62), and Ga (−0.61).

5. Discussion

5.1. Mobility of chemical elements during weathering and gossan evolution

The degree to which the elements migrate before they become relatively fixed in the regolith by adsorption or by precipitation of insoluble minerals is generally referred to as their mobility. The mobility can be complex and multistage with Eh-pH changes, elements solubility, and activity of the complexing agents as major chemical controls (Levinson, 1982; Gray, 2001; Årström and Deng, 2003). In the predominantly oxidizing acid environment typical for the weathering of sulfidic

Table 2
Concentrations of Cu, Zn, δ^{65}Cu and δ^{66}Zn values of analyzed samples of primary ore, gossan, gossan bleached envelope, soils and barren ferruginous crust at the Perkoa area, Burkina Faso.

Sample type and sample code	Cu (ppm)	δ^{65}Cu (‰)	2σ*	Zn (ppm)	δ^{66}Zn (‰)	2σ*
Massive sulfidic ore						
PS200/250.5	536	1.91	0.05	143,600	0.3	0.01
PS200/280.0	147	2.17	0.06	353,900	0.36	0.07
PS200/281.0	250	2.05	0.04	168,500	0.32	0.04
Disseminated sulfidic ore						
PS200/333.54	60.6	0.65	0.01	167	0.63	0.12
PS200/225.9	337.5	0.38	0.01	258	0.17	0.04
PS200/270.3	47.8	0.21	0.02	2455	0.46	0.03
PS200/297.8	49.5	1.73	0.02	534	0.35	0.23
PS200/333.53	34	1.18	0.05	30,400	0.47	0.07
PS200/286.5	171	1.49	0.15	15,700	0.41	0.06
Gossan						
BFPE-2	75	−0.02	0.02	939	−0.099	0.02
BF-PE-8-C	116	−0.58	0.01	1149	−0.27	0.06
BF-PE-8-B	38	−0.15	0.01	500	−0.88	0.06
BF-PE-8-A	56	−0.52	0.02	1151	−0.36	0.04
Bleached envelope of gossan						
BF-PE-23 A	67	−0.62	0.02	1578	−0.46	0.01
BF-PE-21-C	104	−0.49	0.02	1213	0.34	0.04
BF-PE-21-E	23	−0.69	0.09	1300	0.27	0.06
Soil (proximal to gossan)						
BFPE1/1	121	−0.66	0.01	121	−0.63	0.04
BFPE1/2	179	−1.21	0.01	179	−0.61	0.19
Soil (distal to gossan)						
BFPE1/40	34	−0.7	0.01	34	−0.06	0.03
BFPE1/41	40	−1.09	0.01	28	−0.03	0.01
Ferruginous crust						
BFPE9	53	−2.81	0.01	31	−0.36	0.13
BFPE10	49	−2.64	0.01	20	−0.55	0.13
BFPE11	41	−1.82	0.01	17	−0.05	0.12
BFPE12	50	−1.68	0.01	20	−1.05	0.08

* Analyses performed in triplicate.

ores, $Fe_{sulfidic}$, S, Mg, Mn, Ca, Cu, Zn, Ag, Ni, Co, Cd, and Se are very mobile, whereas the mobility of P, As, Ba, Sb, Bi, and especially Pb is low (McQueen, 2008).

This pattern very well corresponds with normalized differences in the geochemistry of primary ores and gossan in the Perkoa deposit (Fig. 13). The relative enrichment and/or depletion of gossan by elements in the studied Perkoa deposit is also in good agreement with the results of investigation of VHMS deposits by other authors (Thornber, 1985; Scott et al., 2001; Velasco et al., 2013; Bartlett et al., 2013; Belogub et al., 2003). Because of the absence of the secondary minerals of Zn, Pb, and Cu, and the predominance of hydro-oxides of iron over other mineral phases (minerals of jarosite group and Mn-oxides) in gossan of the Perkoa deposit, it can be assumed that most of the trace elements, in particular Pb, (Table 1S) in gossan are bound in goethite and hematite. High levels of lead correspond to the relative strengths of metal binding by goethite (Pb > Zn > Co > Ni > Mn) and hematite (McKenzie, 1980). Moreover, goethite and hematite are also an effective anion absorber — particularly of phosphates, sulfates, and arsenates (Eggleton, 2008). Increased concentrations of As_2O_5, P_2O_5, and SO_3 detected in both minerals also correspond to this pattern (Table 1S).

Although goethite and hematite are the most abundant minerals in the studied gossan, part of Pb, As, and P may also be associated with minerals of the alunite supergroup, of which the most common is corkite in the deposit studied. Minerals of this supergroup can also be bearers the rare earth elements (REE). The light rare earth elements (LREE), particularly La and Ce appear to have been the most mobile under the weathering conditions and they may be incorporated into the structure of corkite (Wood, 1990). This corresponds to the La, Ce,

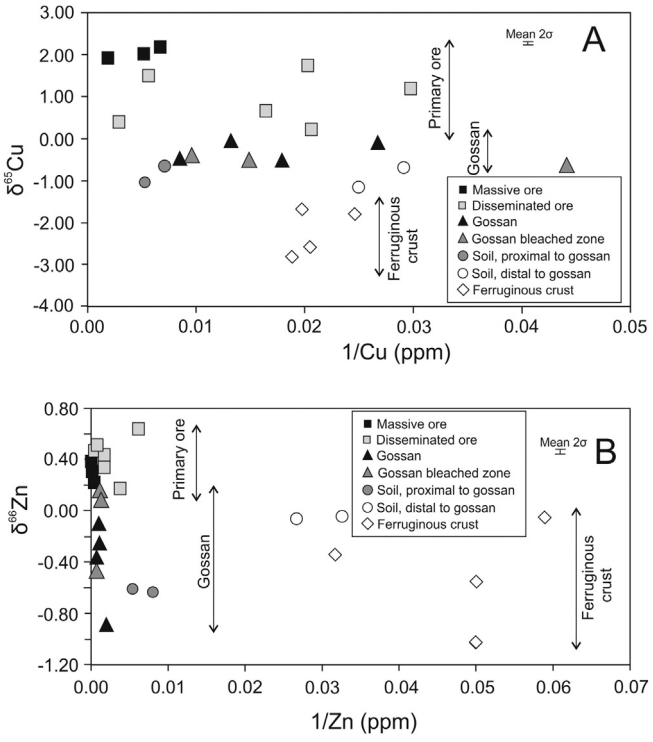

Fig. 17. Concentrations of Cu vs. δ^{65}Cu (A) and zinc vs. δ^{66}Zn (B) in massive and disseminated ore, gossan and in the gossan bleached zone, soil and the barren ferruginous crust in the Perkoa area.

and Pr enrichment in the Perkoa gossan relative to the primary ores (Fig. 14). Brown (1971) showed that minerals of the jarosite supergroup are stable only in the presence of goethite at a pH below 3. The gradually increasing pH, due to the complete dissolution of sulfides, is characteristic of the final (oxidizing and near-neutral) stage of the gossan development. Sulfates in a near-neutral oxidizing environment are not stable being replaced by goethite to form replica textures after subautomorphous minerals of the jarosite supergroup (Fig. 6D). At this stage, a new mobilization of chemical elements bound in minerals of the alunite supergroup may take place including their sorption on minerals of iron. The persistence of minerals of the jarosite supergroup into an environment of higher pH, as was observed in the Perkoa deposit (Fig. 8G), is attributed by Brown (1971) to the slowness of their conversion to goethite or to fluctuations in pH during the process of weathering.

The gossan, compared with abundant hematite and goethite, contains only very low amount of manganese oxides. Although the number of identified Mn minerals in gossan of the Perkoa deposit is very small, a part of Pb, Zn, As, Ba, and S (Table 2S) and even a portion of Cu, Co, Ni, and V may be associated with these Mn minerals (Scott, 1987; Pracejus and Bolton, 1992).

5.2. Discrimination of gossan and the ferruginous crust using multi-element geochemical survey

It is generally agreed that gossan of the volcanic-hosted massive sulfide deposits (VHMS-type), is enriched in As, Ag, Bi, Au, Ba, Cu, Hg, Sb, Se, Sn, and Pb (Taylor and Thornber, 1992). Scott et al. (2001), for example, concluded that Pb is probably the best single pathfinder for VHMS deposits of the eastern Lachlan Fold Belt, Australia, but Ag, As, Au, Bi, Mo, Sb, and Sn are also useful for discrimination. Velasco et al. (2013) reported that gossan capping VHMS deposits in the Iberian Pyrite Belt (Spain) is enriched with Pb, P, Sb, Sn, Ti, Ag, and Au. The Perkoa gossan in comparison with the barren ferruginous crust in the Perkoa area, is enriched in many pathfinders characteristic of VHMS-type deposits

(Ag, As, Ba, Mo, Sb, Pb) — but also in Zn, which is obviously due to the high content of zinc in local ores. High levels of zinc, which is otherwise highly mobile during weathering processes, are also reported in gossan of sediment-hosted, predominantly Zn-rich deposits, (SEDEX-type) in Australia (Bartlett et al., 2013). Even S_{tot} of which high contents in gossan are attributed to the minerals of the alunite supergroup can be included among pathfinder elements at the Perkoa deposit.

5.3. Sources and isotopic fractionation of Pb, Cu, and Zn in supergene processes

5.3.1. Lead isotopes

The isotopic composition of Pb is commonly expressed as ratios $^{206}Pb/^{204}$ Pb, $^{208}Pb/^{204}Pb$ $^{206}Pb/^{207}Pb$, and$^{208}Pb/^{206}Pb$, the $^{208}Pb/^{206}Pb$ vs. $^{206}Pb/^{207}Pb$ plot being the most preferred because it can be precisely determined analytically, and the abundances of these isotopes are relatively important. Furthermore, the abundance of ^{207}Pb (a product of ^{235}U decay) changes very little with time compared to ^{206}Pb (a product of ^{238}U decay) because most ^{235}U was already decayed, while ^{238}U still had a relatively high abundance on the Earth (Erel et al., 2001). For example, while old Pb ores are generally characterized by a low $^{206}Pb/^{207}Pb$ ratio (i.e., Proterozoic Brooken Hill deposit, Austratia: $^{206}Pb/^{207}Pb$ ratios: 1.03–1.10), more recent samples contain more radiogenic Pb (originating from U and Th decay), which is reflected in higher $^{206}Pb/^{207}Pb$ ratios (>1.18; Doe and Delevaux, 1972; Doe and Stacey, 1974; Farmer et al., 2000; Bacon, 2002). Therefore, the $^{206}Pb/^{207}Pb$ ratio of the Perkoa ore (0.98–1.02; Fig. 16) corresponds to the Paleoproterozoic age of this deposit. Compared with Pb ores, isotope composition of soils and ferruginous crusts usually have a higher and more variable $^{206}Pb/^{207}Pb$ ratio, as most of Pb is derived from weathered bedrock minerals (i.e. K-feldspar, up to 1% Pb; micas, up to 100 ppm Pb; Scott, 2008), and the isotopic composition of Pb is mostly influenced by the decay of ^{238}U to ^{206}Pb. Therefore, the $^{206}Pb/^{207}Pb$ ratio in soils widely varies between 1.10 and 1.25, depending of the age and chemical composition of the bedrock (Komárek et al., 2008). As the Pb isotopic signatures are not influenced by weathering (Doe and Stacey, 1974) the gossans and ironstones are readily differentiated isotopically (Gulson and Mizon, 1979; Gulson, 1986). Nevertheless, the results of the Pb isotopic studies at the Perkoa deposit indicate that only gossan has the Pb isotopic composition essentially identical to the primary massive ores. The $^{208}Pb/^{206}Pb$, $^{207}/^{206}Pb$ signature of disseminated mineralization (and the overlapping bleached and argilitized gossan envelope) is not homogenous and probably reflects mixing of "ore lead" with lead derived from the aluminosilicate bedrock. Therefore, when using the Pb isotopes in exploration it is necessary to take into account the character of target mineralization. Studies of the isotopic composition of Pb are likely to be useful in geochemical exploration of ores with high lead content, such as VHMS or SEDEX deposits. When searching for disseminated ores, such as porphyry Cu deposits or orogenic Au deposits the use of Pb isotopes in exploration is likely to be less successful, and isotopic signatures of gossan and the barren ferruginous crust will be very similar, due to the predominance of lithogenic lead over the ore Pb.

5.3.2. Copper isotopes

The whole rock isotopic composition of primary ores at the Perkoa ($\delta^{65}Cu = +0.21$ to $+2.17$‰; Fig. 17A) corresponds to the data of Mathur et al. (2010) who for chalcopyrite/pyrite ores from the primary porphyry Cu deposits in the southwestern United States gave values of $\delta^{65}Cu$ values ranging from -0.9 to $+3.1$‰. A relatively wide range of isotopic values Mathur et al. (2010) explained by the different proportion of chalcopyrite and pyrite in primary ores. According to other authors (Maréchal et al., 1999; Larson et al., 2003; Graham et al., 2004; Rouxel et al., 2004; Mason et al., 2005; Markl et al., 2006; Mathur et al., 2010) the isotopic composition of primary Cu sulfides usually fall within the range 0 ± 1‰ and excursions from this range are attributed to low-temperature secondary processes. When studying gossan (or leached zone) of sulfide deposits, numerous authors state (Mathur et al., 2010,b; Mirnejad et al., 2010) that the oxidation reactions produce large (>1‰) isotopic fractionation of Cu isotopes. This is consistent with our data on Perkoa area where the local gossan and argilitized and bleached rocks related to gossan are on average at 1.71‰ depleted in ^{65}Cu, when compared with primary ores (Table 2, Fig. 17A).

The depletion of sulfides in ^{65}Cu at abiotic low-temperature oxidation were also confirmed by experimental works of many authors such as Mathur et al. (2005), Wall et al. (2006), Kimball et al. (2009), Borrok et al. (2008) and Fernandez and Borrok (2009), in which leachates of primary chalcopyrite or chalcocite were enriched with ^{65}Cu. The depletion of residual phase in ^{65}Cu that occurs during air and aqueous chemical reactions is usually explained as a result of isotopic fractionation caused by electron-exchange-driven Cu(I)/Cu(II) redox reactions on the surface of sulfide minerals (Kimball et al., 2009). Although the valence of Cu in chalcopyrite has been the subject of much debate, the most recent mineralogical studies suggest that the valence state of most Cu in chalcopyrite is Cu(I) (Pearce et al., 2006). During weathering, a thin layer of Cu(II)-sulfate and/or Cu(II)-oxides (in addition to Fe(III)-oxides) commonly develops on the surface of air oxidized chalcopyrite (Pratesi and Cipriani, 2000; Todd et al., 2003). Consistent with this, the experimental evidence shows that redox reactions concentrate ^{65}Cu in the oxidized (and leached) phase as opposed to the residual phase (Ehrlich et al., 2004; Mathur et al., 2005).

The barren ferruginous crust in the area in comparison with gossan of the Perkoa deposit is significantly depleted in ^{65}Cu (Table 2, Fig. 17A). This difference between isotopic composition of Cu in gossan and in the barren ferruginous crust can be explained as a result of synergistic action of several factors: (1) by a different isotopic composition of copper in host rocks compared to its isotopic composition in primary ores, (2) by a multicycle Rayleigh isotope fractionation model, (3) by different intensities of erosion processes, or (4) by action of biogenic elements.

(1) Isotopic composition of Cu in fresh rocks (in volcanic rocks and sediments) usually varies around 0 ± 0.25‰ (Maréchal et al., 1999; Li et al., 2010; Mathur et al., 2012a), and is therefore different from the isotopic composition of copper in primary ores at the Perkoa deposit ($\delta^{65}Cu = +0.21$ to $+2.17$‰). Consequently, it is possible that different values of isotopic composition of copper in ores and in barren rocks are reflected in the isotopic composition of this element in the products of weathering.

(2) According to the simple Rayleigh fractionation model applied to the Cu isotopic fractionation during oxidative leaching by Mathur et al. (2005), a residual phase – for example copper bound in Fe-hydrooxides – is depleted of ^{65}Cu and the resulting solution is ^{65}Cu enriched. The enriched ^{65}Cu solutions migrate downward the rock profile giving rise to the ^{65}Cu-enriched chalcocite or bornite in the supergene enrichment zone. However, due to progressing erosion, the ^{65}Cu -enriched sulfides in the supergene zone are gradually exposed to oxidative alteration, and the resulting isotopic composition of residual phase in gossan reflects a result of isotopic fractionation of both, primary sulfides and ^{65}Cu-enriched supergene sulfides. Consequently, the depletion of residual phase in an oxidative zone of ore deposits is lower, relative to barren rocks (a multicycle Rayleigh isotope fractionation model by Braxton and Mathur, 2011).

(3) Isotopic fractionation of Cu in supergene processes depends both on climatic conditions and also on geographic position of the studied localities. Liu et al. (2014), for example, reported far higher isotopic fractionation of Cu in soils of tropical climates, compared with soils of subtropical climates. Moreover, Palacios et al. (2011) reported that under the same climatic conditions the intensity of isotopic fractionation of copper also depends on the morphology of the terrain. These authors when studying the Pleistocene recycling of Cu in a porphyry system, Atacama,

Chile stated that the leached cap minerals at the highest elevations exhibit relatively more depleted copper isotope signatures than minerals at lower elevations. The authors explained this phenomenon by the fact that the higher elevations experienced greater degrees of oxidative weathering and removal of copper in contrast to areas at lower elevations. This explanation can also be accepted when studying the supergene fractionation of copper in the Perkoa deposit where outcrops of gossan are a part of the lowland which represents the youngest erosion surface of the regolith, while ferrugineous crusts form erosion relics of an older, higher lying well drained erosion surface (Fig. 3). The role of morphology, and hence the intensity of drainage in the fractionation of copper are emphasized by Mathur et al. (2012a) who when studying the weathering of black shales in Pennsylvania (USA) reported that valley topsoils are inclined to be less depleted in ^{65}Cu compared with the ridge topsoils.

(4) Finally, the degree of isotopic fractionation of Cu in supergene processes may also be influenced by biological factors. Previous studies have demonstrated that biological processes could significantly fractionate the Cu isotopes. For example, Cu isotope fractionation has been observed during adsorption of Cu onto cell surfaces, co-precipitation, and adsorption onto mineral coatings (Mathur et al., 2005; Navarete et al., 2011). Zhu et al. (2002) observed Cu isotope variation during its incorporation into proteins synthesized by bacteria and yeast. It can be assumed that a higher biological activity in soils and during the formation of the ferruginous crust compared with limited biological activity during weathering of sulfide ores under conditions of very low pH could have been one of the causes of greater isotopic fractionation of Cu.

5.3.3. Zinc isotopes

Isotopic composition of Zn in ores of the Perkoa deposit ($\delta^{66}Zn = +0.32$ to $+0.36$‰; Table 2, Fig. 17B) is well within the range reported for other ore deposits (-0.72 to $+1.33$‰; Mason et al., 2005; Pichat et al., 2003; Wilkinson et al., 2005). Sonke et al. (2008) proposed a $\delta^{66}Zn$ value of $+0.16 \pm 0.20$‰ for the world average ore-grade sphalerite. Variations in $\delta^{66}Zn$ values for sphalerite in individual ore deposits are relatively small. Wilkinson et al. (2005), for example, found a variation in $\delta^{66}Zn$ of 1.5‰ from single deposits in the Irish Midlands and Mason et al. (2005) reported a 0.66‰ variation from the Alexandrinka volcanic-hosted massive sulfide (VHMS) ore deposit, Urals, Russia.

The fractionation of Zn isotopes during sulfide weathering is relatively small compared to Cu, probably because Zn, unlike Cu, is not a redox-sensitive element. The depletion in ^{66}Zn during sphalerite weathering is explained by the formation of Zn-sulfates surface coatings (Steger and Desjardins, 1980) that preferentially incorporate the heavier Zn isotope (Fernandez and Borrok, 2009). The removal of the heavier Zn isotope during the experimental leaching of sphalerite (Fernandez and Borrok, 2009; Matthies et al., 2014) revealed that the leachate isotopic signature reach a maximum offset of $+0.32$‰ compared to the original sphalerite isotope signature.

At the Perkoa deposit, however, the depletion of gossan in ^{66}Zn is higher (median $\Delta^{66}Zn_{gossan-massive\ ore}$: -0.73‰, Fig. 17), and very variable. This can be explained either by Zn that is released not only from sphalerite but also from other different mineral phases, such as carbonates or ferromagnesian minerals in ore or the isotopic composition of Zn in the process of weathering is modified due to variable speciation (Maréchal and Albarède, 2002), adsorption on organic and inorganic surfaces (Weiss et al., 2005; Pokrovsky et al., 2005; Gélabert et al., 2006), ion exchange (Maréchal and Albarède, 2002), diffusion (Rodushkin et al., 2004), or by the uptake by microorganisms and higher plants (Archer and Vance, 2002; Albarède, 2004; Weiss et al., 2005; Bermin et al., 2006; Gélabert et al., 2006). Weiss et al. (2002, 2005) reported, for example, that the lighter Zn isotope is preferentially taken during the plant uptake. The combination of all these factors apparently causes the isotopic composition of Zn in products of weathering of sulfide ores (i.e. in gossan and in gossan bleached envelope) in principle does not differ from isotopic composition of Zn in soils and in regional ferruginous crust (Fig. 17B).

6. Conclusions

The mature gossan of the Paleoproterozoic VHMS-type deposit of Perkoa in Burkina Faso consists predominantly of hematite and goethite, with an admixture of hydrous Mn-phase, minerals of the alunite supergroup (corkite, hinsdalite, and hidalgonite), and clay minerals.

Results of the present study revealed that gossan differs from lateritic soils and especially from the barren ferruginous crust in the same area in: (1) the preservation of hematite and goethite pseudomorphs after sulfides, (2) the presence of barite, sphalerite, and cinnabar enclosed in residual quartz grains, (3) elevated contents of many trace elements, particularly As, Pb, Sb, and Zn, and to less extent also of Ag, Ba Cd, Mo, and Sr. High contents of Zn, i.e. the element which is not a typical pathfinder for the VHMS-type deposits is due to the predominance of zinc over copper and lead in primary ores. The content of S_{tot} is also elevated which mirrors the occurrence of the jarosite supergroup minerals.

Gossan and the barren ferruginous crust differ in the isotope composition of Pb and Cu. The $^{206}Pb/^{207}Pb$ and $^{208}Pb/^{206}Pb$ ratios in gossan are identical with the same ratios in massive sulfidic ores. However, the isotopic composition of Pb in disseminated ores and the bleached gossan envelope are more variable, most probably due to mixing of ore and lithogenic lead. Compared with the ferruginous crust, the gossan is less depleted in ^{65}Cu. In contrast to the isotopic composition of Pb and Cu, the isotopic composition of Zn in gossan and the ferruginous crust is similar, which can be explained as due to high mobility of Zn, small changes in Zn isotopic composition, and many factors affecting the isotopic composition of Zn in supergenous processes.

The results show that the study of mineralogy of gossan in combination with multi-elemental geochemical methods and investigation of isotopic composition of lead and copper are an effective tool to distinguish mineralized and barren weathered protoliths.

Supplementary data to this article can be found online at http://dx.doi.org/10.1016/j.gexplo.2016.05.007.

Acknowledgments

This study was carried out within the P934A – West Africa exploration initiative – Stage 2 (@ AMIRA International) program and by the Operational Program Prague – Competitiveness (Project CZ.2.16/3.1.00/21516). The authors are grateful to Messrs. Adama Barry and Ibrahim Banao of the Nantou Mining Company for providing materials for this study, and for their guidance around the Perkoa deposit. We would like to thank Lucie Erbanová (Czech Geological Survey) for carrying out isotope analyses of zinc in the early stage of the project. The authors are indebted to Jaroslav Hak for English editing. The manuscript substantially benefited from the comments of Ryan Mathur (Juniata College, Huntingdon, Pennsylvania), anonymous reviewer, and from those of Arnold Justus Stanly, Journal of Geochemical Exploration Manager.

References

Albarède, F., 2004. The Stable Isotope Geochemistry of Copper and Zinc. In: Johnson, C.M., Beard, B.L., Albarède, F. (Eds.), Geochemistry of Nontraditional Stable Isotopes: Reviews in Mineralogy vol. 55. Mineralogical Society of America, pp. 409–427.

Andrew, R.L., 1984. The geochemistry of selected base-metal gossans, Southern Africa. J. Geochem. Explor. 22, 161–192.

Archer, C., Vance, D., 2002. Large fractionations in Fe, Cu and Zn isotopes associated with Archean microbially-mediated sulfides. Geochim. Cosmochim. Acta 66 (S1), A26.

Årström, M., Deng, H., 2003. Assessment of the mobility of trace elements in acidic soils using soil and stream geochemical data. Geochem. Explor. Environ. Anal. 3, 197–203.
Atapour, H., Aftabi, A., 2007. The geochemistry of gossans associated with Sarcheshmeh porphyry copper deposit, Rafsanjan, Kerman, Iran: Implications for exploration and the environment. J. Geochem. Explor. 93, 47–65.
Bacon, J.R., 2002. Isotopic characterisation of lead deposited 1989–2001 at two upland Scottish locations. J. Environ. Monit. 4, 291–299.
Bartlett, R., Jenkin, G.R.T., Plimer, I.R., 2013. Re-examination of the Broken Hill gossan: applications to exploration for Broken Hill-type mineralization. In: Jonsson, E. (Ed.), Mineral Deposit Research for a High-Tech World12th Biennial SGA Meeting Uppsala, Sweden. Geological Survey of Sweden, Uppsala, pp. 400–402.
Bayliss, P., Kolitsch, U., Nickel, E.H., Pring, A., 2010. Alunite supergroup: recommended nomenclature. Mineral. Mag. 74, 919–927.
Belogub, E.V., Novosedlov, C.A., Spiro, B., Yakovleva, A., 2003. Mineralogical and S isotopic features of the supergene profile of the Zapadno-Ozernoe massive sulfide and Au-bearing gossan deposit, South Urals. Mineral. Mag. 67, 339–354.
Bermin, J., Vance, D., Archer, C., Statham, P.J., 2006. The determination of the isotopic composition of Cu and Zn in seawater. Chem. Geol. 226, 280–297.
Béziat, D., Dubois, M., Debat, P., Nikiema, S., Salvi, S., Tollon, F., 2008. Gold metallogeny in the Birimian craton of Burkina Faso (West Africa). J. Afr. Earth Sci. 50, 215–233.
Blot, A., 2004. Caractérisation des chapeaux de fer en milieu latéritique cuirassé. Compt. Rendus Geosci. 336, 1473–1480.
Borrok, D.M., Nimick, D.A., Wanty, R.B., Ridley, W.I., 2008. Isotopic variations of dissolved copper and zinc in stream waters affected by historical mining. Geochim. Cosmochim. Acta 72, 329–344.
Boyle, D.R., 1994. Oxidation of massive sulfide deposits in the Bathurst mining camp, New Brunswick – Natural analogs for acid drainage in temperate climates. In: Alpers, C.N., Blowes, D.W. (Eds.), Environmental Geochemistry of Sulfide Oxidation. ACS Symposium Series Vol. 550, pp. 535–550.
Braun, J.J., Pagel, M., 1990. U, Th and REE in the Akongo lateritic profil (SW Cameroon). Chem. Geol. 84, 357–359.
Braxton, D., Mathur, R., 2011. Exploration applications of copper isotopes in the supergene environment: A case study of the Bayugo porphyry copper-gold deposit, southern Philippines. Econ. Geol. 106, 1447–1463.
Brown, J.B., 1971. Jarosite-goethite stabilities at 25 °C, 1 ATM. Mineral. Deposita 6, 245–252.
Burke, K., Gunnell, Y., 2008. The African erosion surface: a continental-scale synthesis of geomorphology, tectonics, and environmental change over the past 180 million years. Geol. Soc. Am. Mem. 201, 80.
Butt, C.R.M., Robertson, D.M., Scott, K.M., Cornelius, M. (Eds.), 2005. Regolith Expression of Australian Ore Systems. CSIRO Publishing.
Butt, C.R.M., Scott, K.M., Cornelius, M., Robertson, D.M., 2008. Regolith sampling for geochemical exploration. In: Scott, K.K., Pain, C.F. (Eds.), Regolith Science. Springer Science and CSIRO Publishing, pp. 341–376.
Chardon, D.V., Chevillotte, A., Beauvais, A., Grandin, G., Boulangé, B., 2006. Planation, bauxites and epeirogeny: One or two paleosurfaces on the West African margin? Geomorphology 82, 273–282. http://dx.doi.org/10.1016/j.geomorph.2006.05.008.
Dempírová, L., Vitková, H., 2002. Methods of Certified Chemical Analyses (MS.) Czech Geological Survey, Prague (in Czech with English summary).
Doe, B.R., Delevaux, M.H., 1972. Source of lead in Southeast Missouri galena ores. Econ. Geol. 67, 409–425.
Doe, B.R., Stacey, J.S., 1974. Application of lead isotopes to problems of ore genesis and ore prospect evaluation. Econ. Geol. 69, 757–776.
Egal, E., Thiéblemont, D., Lahondère, D., Guerrot, C., Costea, C.A., Iliescu, D., Delor, C., Goujou, J.-C., Lafon, J.M., Tegyey, M., 2002. Late Eburnean granitization and tectonics along the western and northwestern margin of the Archean Kenema-Man domain (Guinea, West African Craton). Precambrian Res. 117, 57–84.
Eggleton, R.A., 2008. Regolith mineralogy. In: Scott, K.M., Pain, C.F. (Eds.), Regolith Science. Springer Science and CSIRO Publishing, pp. 45–72.
Ehrlich, S., Butler, I., Halicz, L., Rickard, D., Oldroyd, A., Matthews, A., 2004. Experimental study of the copper isotope fractionation between aqueous Cu(II) and covellite, CuS. Chem. Geol. 209, 259–269.
Emmons, W.H., 1917. The enrichment of ore deposits. Bull. US Geol. Surv. 625 (530 pp.).
Erel, Y., Dubowski, Y., Halicz, L., Erez, J., Kaufman, A., 2001. Lead concentrations andisotopic ratios in the sediments of the sea of Galilee. Environ. Sci. Technol. 35, 292–299.
Ettler, V., Mihaljevič, M., Komárek, M., 2004. ICP-MS measurements of lead isotopic ratios in soils heavily contaminated by lead smelting: tracing the sources of pollution. Anal. Bioanal. Chem. 378, 311–317.
FAO, 2006. Guidelines for Soil Description. Food and Agriculture Organization of the United Nations, Rome.
Farmer, J.G., Eades, L.J., Graham, M.C., Bacon, J.R., 2000. The changing nature of the Pb-206/Pb-207 isotopic ratio of lead in rainwater, atmospheric particulates, pine needles and leaded gasoline in Scotland, 1982–1998. J. Environ. Monit. 2, 49–57.
Fernandez, A., Borrok, D.M., 2009. Fractionation of Cu, Fe, and Zn isotopes during the oxidative weathering of sulfide-rich rocks. Chem. Geol. 264, 1–12.
Feybesse, J.L., Milési, J.P., 1994. The Archean/proterozoic contact zone in West Africa: a mountain belt of décollement thrusting and folding on a continental margin related to 2.1 Ga convergence of Archean cratons? Precambrian Res. 69, 199–227.
Feybesse, J.L., Billa, M., Guerrot, C., Duguey, E., Lescuyer, J.L., Milési, J.P., Bouchot, V., 2006. The paleoproterozoic Ghanaian province: geodynamic model and ore controls, including regional stress modeling. Precambrian Res. 149, 149–196.
Gélabert, A., Pokrovsky, O.S., Viers, J., Schott, J., Boudou, A., Feurtet-Mazel, A., 2006. Interaction between zinc andfreshwater and marine diatom species: surface complexationand Zn isotope fractionation. Geochim. Cosmochim. Acta 70, 839–857.
Graham, S., Pearson, N., Jackson, S., Griffin, W., O'Reilly, S.Y., 2004. Tracing Cu and Fe from source to porphyry: in situ determination of Cu and Fe isotope ratios in sulfides from the Grasberg Cu–Au deposit. Chem. Geol. 207, 147–169.
Grandin, G., 1976. Aplanissements cuirassés et enrichissement des gisements de manganèse dans quelques régions d'Afrique de l'Ouest. Mém. ORSTOM 82 (276 pp.).
Gray, D.J., 2001. Hydrogeochemistry in the Yilgarn Craton. Geochem. Explor. Environ. Anal. 1, 253–264.
Gulson, B.L., 1986. Lead Isotopes in Mineral Exploration. Elsevier, Amsterdam.
Gulson, B.L., Mizon, K.J., 1979. Lead isotopes as a tool for gossan assessment in base metal exploration. J. Geochem. Explor. 11, 299–320.
Kimball, B.E., Mathur, R., Dohnalkova, A.C., Wall, A.J., Runkel, R.L., Brantley, S.L., 2009. Copper isotope fractionation in acid mine drainage. Geochim. Cosmochim. Acta 73, 1247–1263.
Komárek, M., Ettler, V., Chrastný, V., Mihaljevič, M., 2008. Lead isotopes in environmental sciences: A review. Environ. Int. 34, 562–577.
Larson, P.B., Maher, K., Ramos, F.C., Chang, Z., Gaspar, M., Meinert, L.D., 2003. Copper isotope ratios in magmatic and hydrothermal ore-forming environments. Chem. Geol. 201, 337–350.
Ledru, P., Johan, V., Milési, J.P., Tegyey, M., 1991. Transcurrent tectonics and polycyclic evolution in the lower Proterozoic of Senegal-Mali. Precambrian Res. 50, 337–354.
Ledru, P., Johan, V., Milési, J.P., Tegyey, M., 1994. Markers of the last stages of the Palaeoproterozoic collision: evidence for a 2 Ga continent involving circum-South Atlantic provinces. Precambrian Res. 69, 169–191.
Levinson, A.A., 1982. Introduction to Exploration Geochemistry. second ed. Applied Publishing Ltd., Wilmette.
Li, W., Jackson, S.E., Pearson, N.J., Graham, S., 2010. Copper isotopic zonation in the Northparkes porphyry Cu-Au deposit SE Australia. Geochim. Cosmochim. Acta 74, 4078–4096.
Liégeois, J.P., Claessens, W., Camara, D., Klerkx, J., 1991. Short-lived Eburnian orogeny in southern Mali. Geology, tectonics, U-Pb and Rb-Sr geochronology. Precambrian Res. 50, 111–136.
Liu, S.-A., Teng, F.-Z., Li, S., Wei, G.-J., Ma, J.-L., Li, D., 2014. Copper and irpn isotope fractionation during weathering and pedogenesis: Insight from saprolite profiles. Geochim. Cosmochim. Acta 146, 59–75.
Maréchal, C.N., Albarède, F., 2002. Ion-exchange fractionation of copper and zinc isotopes. Geochim. Cosmochim. Acta 66, 1499–1509.
Maréchal, C.N., Télouk, P., Albaréde, F., 1999. Precise analysis of copper and zinc isotopic compositions by plasma-source mass spectrometry. Chem. Geol. 156, 251–273.
Markl, G., Lahaye, Y., Schwinn, G., 2006. Copper isotopes as monitors of redox processes in hydrothermal mineralization. Geochim. Cosmochim. Acta 70, 4215–4228.
Mason, T.F.D., Weiss, D.J., Chapman, J.B., Wilkinson, J.J., Tessalina, S.G., Spiro, B., Horstwoodd, M.S.A., Spratt, J., Coles, B.J., 2005. Zn and Cu isotopic variability in the Alexandrinka volcanic-hosted massive sulfide (VHMS) ore deposit, Urals, Russia. Chem. Geol. 221, 170–187.
Mathur, R., Ruiz, J., Titley, S., Liermann, L., Buss, H., Brantley, S., 2005. Cu isotopic fractionation in the supergene environment with and without bacteria. Geochim. Cosmochim. Acta 69, 5233–5246.
Mathur, R., Dendas, M., Titley, S., Phillips, A., 2010. Patterns in the copper isotope composition of minerals in porphyry copper deposits in southwestern United States. Econ. Geol. 105, 1457–1467.
Mathur, R., Jin, L., Prush, V., Paul, J., Ebersole, C., Fornadel, A., Williams, J.Z., Brantley, S., 2012a. Cu isotopes and concentrations during weathering of black shale of the Marcellus formation, Huntingdon County, Pennsylvania (USA). Chem. Geol. 304-305, 175–184.
Mathur, R., Ruiz, J., Casselman, M.J., Megaw, P., van Egmond, R., 2012b. Use of Cu isotopes to distinguish primary and secondary Cu mineralization in the Cañariaco Norte porphyry copper deposit, Northern Peru. Mineral. Deposita 47, 755–762.
Matthies, R., Krahé, L., Blowes, D.W., 2014. Zinc stable isotope fractionation upon accelerated oxidative weathering of sulfidic mine waste. Sci. Total Environ. 487, 97–101.
McKenzie, R.M., 1980. The adsorption of lead and other heavy metals on oxides of manganese and iron. Aust. J. Soil Res. 18, 61–73.
McQueen, K., 2008. Regolith geochemistry. In: Scott, K.M., Pain, C.F. (Eds.), Regolith Science. Springer Science and CSIRO Publishing, pp. 74–104.
Michel, P., 1973. Les bassins des fleuves Sénégal et Gambie: étude géomorphologique. Mém. ORSTOM 63 (383 pp. (in French with English abstract)).
Mihaljevič, M., Ettler, V., Šebek, O., Sracek, O., Kříbek, B., Kyncl, T., Majer, V., Veselovský, F., 2011. Lead isotopic and metallic pollution record in tree rings from the Copperbelt mining-smelting area. Zambia. Water Air Soil Pollut. 216, 657–668.
Milési, J.P., Feybesse, J.L., Ledru, P., et al., 1989. Minéralizations aurifères 1009 de l'Afrique de l'ouest. Leur relations avec l'evolution litho-structurale au Protérozoïque inférieur. Carte géologique au 1 / 2.000.000. Chron. Rech. Min. 497, 3–98 (in French with English abstract).
Milési, J.-P., Ledru, P., Feybesse, J.-L., Dommanget, A., Marcoux, E., 1992. Early Proterozoic ore deposits and tectonics of the Birimian orogenic belt, West Africa. Precambrian Res. 58, 305–344.
Milési, J.P., Feybesse, J.L., Pinna, P., Deschamps, Y., Kampunzu, H., Muhongo, S., Lescuyer, J.L., Le Goff, E., Delor, C., Billa, M., Ralay, F., Heinry, C., 2004. Geological map of Africa 1:10,000,000, SIG Afrique project. In: 20th Conference of African Geology, BRGM, Orléans, France, 2–7 June, http://www.sigafrique.net (last accessed 1016 14/12/2013).
Mirnejad, H., Mathur, R., Einali, M., Dendas, M., Alirezaei, S., 2010. A comparative copper isotope study of porphyry copper deposits in Iran. Geochem. Explor. Environ. Anal. 10, 413–418.
MTMCI (Mining Technology Market & Customer Insight), 2015. The Perkoa zinc mine, Sanguie. http://www.mining-technology.com/projects/-perkoa-zinc-mine-BurkinaFaso (Visited 05.05.2015).

Navarete, J.U., Borrok, D.M., Viveros, M., Ellzey, J.T., 2011. Copper isotope fractionation during surface adsorption and intracellular incorporation by bacteria. Geochim. Cosmochim. Acta 75, 784–799.
Palacios, C., Rouxel, O., Reich, M., Cameron, E., Leybourne, M., 2011. Pleistocene recycling of copper at a porphyry system, Atacama Desert, Chile: Cu isotope evidence. Mineral. Deposita 46, 1–7. http://dx.doi.org/10.1007/s00126-010-0315-6.
Pearce, C.I., Pattrick, R.A.D., Vaughan, D.J., Henderson, C.M.B., van der Laan, G., 2006. Copper oxidation state in chalcopyrite: mixed Cu d9 and d10 characteristics. Geochim. Cosmochim. Acta 70, 4635–4642.
Pichat, S., Douchet, C., Albarede, F., 2003. Zinc isotope variations in deep-sea carbonatesfrom the eastern equatorial Pacific over the last 175 ka. Earth Planet. Sci. Lett. 210, 167–178.
Pokrovsky, O.S., Viers, J., Freydier, R., 2005. Zinc stable isotope fractionation during its adsorption on oxides and hydroxides. J. Colloid Interface Sci. 291, 192–200.
Pracejus, B., Bolton, B.R., 1992. Geochemistry of supergene manganese oxide deposits, Groote Eylandt, Australia. Econ. Geol. 87, 1310–1335.
Pratesi, G., Cipriani, C., 2000. Selective depth analyses of the alteration products of bornite, chalcopyrite and pyrite performed by XPS, AES, RBS. Eur. J. Mineral. 12, 397–409.
Rodushkin, I., Stenberg, A., André, H., Maklinovsky, D., Baxter, D.C., 2004. Isotopic fractionation during diffusion of transition metal ions in solution. Anal. Chem. 76, 2148–2151.
Rouxel, O., Fouquet, Y., Ludden, J.N., 2004. Copper isotope systematics of the lucky strike, rainbow, and Logatchev sea-floor hydrothermal fields on the Mid-Atlantic Ridge. Econ. Geol. 99, 585–600.
Schwartz, M.O., Melcher, F., 2003. The Perkoa zinc deposit, Burkina Faso. Econ. Geol. 98, 1463–1485.
Scott, K.M., 1987. Solid solution in, and classification of, gossan-derived members of the alunite-jarosite family, northwest Queensland, Australia. Am. Mineral. 72, 178–187.
Scott, K.M., 2008. Regolith geochemistry of elements. In: Scott, K.M., Pain, C.F. (Eds.), Regolith Science. Springer Science and CSIRO Publishing, pp. 433–452.
Scott, K.M., Ashley, P.M., Lawie, D.C., 2001. The geochemistry, mineralogy and maturity of gossans derived from volcanogenic Zn-Pb-Cu deposits of the eastern Lachlan Fold Belt, NSW, Australia. J. Geochem. Explor. 72, 169–191.
Séranne, M., 1999. Early Oligocene stratigraphy turnover on the West Africa continental margin: a signature of the tertiary greenhouse-to-icehouse transition? Terra Nova 11, 135–140.
Skarpelis, N., Argyraki, A., 2009. Geology and origin of supergene supergene ore at the Lavrion Pb-Ag-Zn deposit, Attica, Greece. Resour. Geol. 59, 1–14.
Sonke, J.E., Sivry, Y., Viers, J., Freydier, R., Dejonghe, L., André, L., Aggarwal, J.K., Fontan, F., Dupré, B., 2008. Historical variations in the isotopic composition of atmospheric zinc deposition from a zinc smelter. Chem. Geol. 252, 145–157.
Steger, H.F., Desjardins, L.E., 1980. Oxidation of sulfide minerals; V, galena, sphalerite and chalcocite. Can. Mineral. 18, 365–372.
Taylor, G.F., Thornber, M.R., 1992. Gossan and ironstone surveys. In: Butt, C.R.M., Zeegers, H. (Eds.), Regolith Exploration Geochemistry in Tropical and Subtropical TerranesHandbook of Exploration Geochemistry vol. 4. Elsevier, Amsterdan, pp. 139–202.
Taylor, G.F., Wilmshurst, J.R., Butt, C.R.M., Smith, R.E., 1980. Gossans. J. Geochem. Explor. 22, 30–32.
Thornber, M.R., 1985. Supergene alteration of sulfides: VII. Distribution of elements during the gossan-forming process. Chem. Geol. 53, 279–301.
Todd, E.C., Sherman, D.M., Purton, J.A., 2003. Surface oxidation of chalcopyrite (CuFeS2) under ambient atmospheric and aqueous (pH 2–10) conditions: Cu, Fe land O K-edge X-ray spectroscopy. Geochim. Cosmochim. Acta 67, 2137–2146.
USGS, 1998. Certificate of Analysis. Andesite, AGV 2 1998; U.S. Geological Survey Open-File Report, Denver.
Vaasjoki, M., 1985. The Teutonic Bore deposit, Western Australia – A lead isotope study of an ore and its gossan. Mineral. Deposita 20, 266–270.
Velasco, F., Herrero, J.M., Suárez, S., Yusta, I., Alvaro, A., Tornos, F., 2013. Supergene features and evolution of gossans capping massive sulfide deposits in the Iberian Pyrite Belt. Ore Geol. Rev. 53, 181–203.
Voldřichová, P., Chrastný, V., Šípková, A., Farkaš, J., Novák, M., Štěpánová, M., Krachler, M., Veselovský, F., Bláha, V., Přechová, E., Komárek, A., Bohdálková, L., Čuřík, J., Míková, J., Erbanová, L., Pacherová, P., 2014. Zinc isotope systematics in snow and ice accretions in Central European Mountains. Chem. Geol. 388, 130–141.
Wall, A., Heaney, P.J., Mathur, R., Jeffrey, E., 2006. Copper Isotope Fractionation during Theoxidative Phase Transition of Sulfide Minerals, Chalcocite to Covellite, Using Time-Resolved Synchrotron X-Ray Diffraction. GSA Abstracts with Programs Vol. 38 p. 432.
Weiss, D., Shotyk, W., Page, S.E., Rieley, J.O., Reese, S., Martinez-Cortizas, A., 2002. The geochemistry of major and selected trace elements in a forested peat bog, Kalimantan, SE-Asia, and its implications on past atmospheric dust deposition. Geochim. Cosmochim. Acta 66, 2307–2323.
Weiss, D.J., Mason, T.F.D., Zhao, F.J., Kirk, G.J.D., Coles, B.J., Horstwood, M.S.A., 2005. Isotopic discrimination of Zn in higher plants. New Phytol. 165, 703–710.
Wilkinson, J.J., Weiss, D.J., Mason, T.F.D., Coles, B.J., 2005. Zinc isotope variation inhydrothermal systems: preliminary evidence from the Irish Midlands Ore field. Econ. Geol. 100, 583–590.
Williams, P.A., 1990. Oxide Zone Geochemistry. Ellis Harwood, New York (286 pp.).
Wood, S.A., 1990. The aqueous geochemistry of the rare earth elements and yttrium. Review of available low-temperature data for inorganic complexes and the inorganic REE speciation of natural waters. Chem. Geol. 82, 159–186.
Zhu, X.K., Guo, Z., Williams, R.J.P., O'Nions, R.K., Matthews, A., Belshaw, N.S., Canters, G.W., De Waal, E.C., Weser, U., Burgess, B.K., Salvato, B., 2002. Mass fractionation processes of transition metal isotopes. Earth Planet. Sci. Lett. 200, 47–62.
Zida, B., 2002. Burkina Faso: Mining Annual Review 2002 (CD-ROM).